

Journal Pre-proof

An attempt to chemically state the cross-talk between monomers of COX homodimers by double/hybrid inhibitors mofezolac-spacer-mofezolac and mofezolac-spacer-arachidonic acid

Maria Grazia Perrone, Morena Miciaccia, Paola Vitale, Savina Ferorelli, Cristina da Costa Bernardes Araújo, Gabriella Silva de Almeida, Thaisa Francielle Souza Domingos, Luiz Claudio Rodrigues Pereira da Silva, Marcelo de Pádula, Lucio Mendes Cabral, Plínio Cunha Sathler, Carmela Bonaccorso, Cosimo G. Fortuna, Antonio Scilimati

PII: S0223-5234(20)30891-6

DOI: <https://doi.org/10.1016/j.ejmech.2020.112919>

Reference: EJMECH 112919

To appear in: *European Journal of Medicinal Chemistry*

Received Date: 3 July 2020

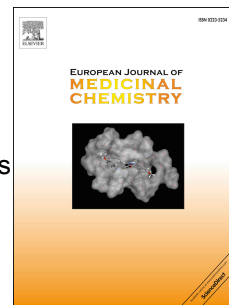
Revised Date: 18 September 2020

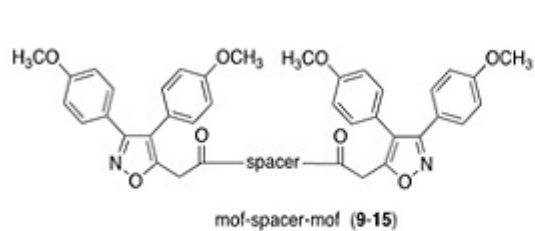
Accepted Date: 5 October 2020

Please cite this article as: M.G. Perrone, M. Miciaccia, P. Vitale, S. Ferorelli, C. da Costa Bernardes Araújo, G. Silva de Almeida, T.F. Souza Domingos, L.C. Rodrigues Pereira da Silva, M. de Pádula, L.M. Cabral, P.C. Sathler, C. Bonaccorso, C.G. Fortuna, A. Scilimati, An attempt to chemically state the cross-talk between monomers of COX homodimers by double/hybrid inhibitors mofezolac-spacer-mofezolac and mofezolac-spacer-arachidonic acid, *European Journal of Medicinal Chemistry*, <https://doi.org/10.1016/j.ejmech.2020.112919>.

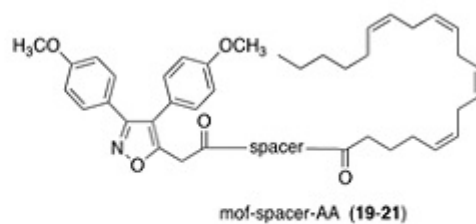
This is a PDF file of an article that has undergone enhancements after acceptance, such as the addition of a cover page and metadata, and formatting for readability, but it is not yet the definitive version of record. This version will undergo additional copyediting, typesetting and review before it is published in its final form, but we are providing this version to give early visibility of the article. Please note that, during the production process, errors may be discovered which could affect the content, and all legal disclaimers that apply to the journal pertain.

© 2020 Published by Elsevier Masson SAS.





COX-1 IC₅₀ 0.013 - 15 μM
COX-2 IC₅₀ 0.05 - 17 μM



COX-1 IC₅₀ 0.05 - 17 μM
COX-2 IC₅₀ 0.09 - >50 μM

Journal Pre-proof

An attempt to chemically state the cross-talk between monomers of COX homodimers by double/hybrid inhibitors mofezolac-spacer-mofezolac and mofezolac-spacer-arachidonic acid

Maria Grazia Perrone^a, Morena Miciaccia^a, Paola Vitale^a, Savina Ferorelli^a, Cristina da Costa Bernardes Araújo^b, Gabriella Silva de Almeida^b, Thaisa Francielle Souza Domingos^b, Luiz Claudio Rodrigues Pereira da Silva^b, Marcelo de Pádula^b, Lucio Mendes Cabral^b, Plínio Cunha Sathler^b, Carmela Bonaccorso^c, Cosimo G. Fortuna^c, Antonio Scilimati^{a,*}

^aDepartment of Pharmacy - Pharmaceutical Sciences, University of Bari “Aldo Moro”, Via E. Orabona 4, 70125, Bari, Italy. ^bFaculty of Pharmacy, Federal University of Rio de Janeiro, Center of Health Sciences, Carlos Chagas Filho Avenue, 373, 21941599, Rio de Janeiro, Brazil.

^cDepartment of Chemical Science, University of Catania, Viale Andrea Doria 6, 95125, Catania, Italy.

Corresponding author: Antonio Scilimati phone, +39 080 5442753; fax, +39 080 5442724, email: antonio.scilimati@uniba.it.

ABSTRACT

Cardiovascular diseases (CVDs) account for over 17 million death globally each year, including arterial thrombosis. Platelets are key components in the pathogenesis of this disease and modulating their activity is an effective strategy to treat such thrombotic events. Cyclooxygenase-1 (COX-1) isoenzyme is involved in platelet activation and is the main target of non-steroidal anti-inflammatory drugs (NSAIDs) and new selective inhibitor research. Such inhibitors of general formula mofezolac-spacer-mofezolac (mof-spacer-mof) and mofezolac-spacer-arachidonic acid (mof-spacer-AA) were projected to investigate the possible cross-talk between the two monomers (E_{allo} and E_{cat}) forming the COX-1 homodimer. Mofezolac was chosen as either one or two moieties of these molecules being the known most potent and selective COX-1 inhibitor and administered to humans as Disopain™, then arachidonic acid (AA) was used to develop molecules bearing, in the same compound, in addition to the inhibitor moiety (mofezolac) also the natural COX substrate. Depending on the nature of the spacer, COX-1 and COX-2 activity was differently inhibited by mof-spacer-mof set with a preferential COX-1 inhibition. The highest COX-1 selectivity was exhibited by the compound in which the spacer was the benzidine [*N,N'*-(biphenyl-4,4'-di-yl)bis(2-(3,4-bis(4-methoxyphenyl)isoxazol-5-yl)acetamide) (**15**): COX-1 IC_{50} = 0.08 μM , COX-2 IC_{50} > 50 μM , Selectivity Index (SI) > 625]. In the case of mof-spacer-AA set, the COX inhibitory potency and also the isoform preference changed. (5Z, 8Z, 11Z, 14Z)-*N*-(4-{2-[3,4-Bis(4-methoxyphenyl)isoxazol-5-yl]acetamido}butyl)icosa-5,8,11,14-tetraenamide (**19**) and (5Z, 8Z, 11Z, 14Z)-*N*-(4'-{2-[3,4-bis(4-methoxyphenyl)isoxazol-5-yl]acetamido}-[1,1'-biphenyl]-4-yl)icosa-5,8,11,14-tetraenamide (**21**), in which the spacer is the 1,2-diaminobutane or benzidine, respectively, selectively inhibited the COX-2, whereas when the spacer is the 1,4-phenyldiamine [(5Z, 8Z, 11Z, 14Z)-*N*-(4-{2-[3,4-bis(4-methoxyphenyl)isoxazol-5-yl]acetamido}phenyl)icosa-5,8,11,14-tetraenamide) (**20**) the COX preference is COX-1 (COX-1

$IC_{50} = 0.05 \mu\text{M}$, COX-2 $IC_{50} > 50 \mu\text{M}$, with a COX-1 selectivity > 1000). Molecular modelling by using FLAP algorithm shows fundamental interactions of the novel compounds at the entry channel of COX and inside its catalytic cavity. The effect of these mof-spacer-mof and mof-spacer-AA in inhibiting *in vitro* free arachidonic acid-induced platelet aggregation was also determined. A positive profile of hemocompatibility in relation to their influence on the blood coagulation cascade and erythrocyte toxicity was observed. Cytotoxicity and genotoxicity safety were also found for these two novel sets of compounds.

KEYWORDS: Mofezolac, Arachidonic acid, COX-1 and COX-2 selective inhibitors, Fingerprints for Ligands and Proteins, Drug design, Antiplatelet agents, Thrombosis, Cardiovascular diseases

1. Introduction

According to World Health Organization (WHO), cardiovascular diseases (CVDs) are responsible to 17.7 million deaths worldwide per year, representing 31% of all deaths. This number is expected to grow to 23.6 million until 2030^{1,2}. Atherosclerosis is the most common clinical manifestation related to CVDs, which is characterized by an atherosclerotic plaque accumulation causing arterial wall thickening and luminal narrowing^{1,3}. Rupture of atherosclerotic plaques in vessels may cause thrombotic occlusion leading to a myocardial infarction and ischemic stroke^{4,5}.

Platelets play a key role in pathogenesis of atherothrombosis due to their ability of aggregation and adhesion in the content of atherosclerotic plaques exposed in arterial circulation after rupture, forming with them a thrombus rich in fibrin⁶⁻⁸. Antiplatelet therapy, such as clopidogrel and aspirin, is used for treatment and prevention of atherothrombosis⁹. Aspirin is a drug that act as an irreversible inhibitor of both COX-1 and COX-2, and at low dose selectively inhibits COX-1^{9,10}. COX-1 is an enzyme present also in platelet surface, where it is responsible to oxidize the arachidonic acid (AA), its natural substrate, leading to the thromboxane A₂ (TXA₂) formation, which is in turn a platelet activator and increases the platelet aggregation¹¹. Therefore, COX-1 inhibitors are used as antiplatelets, reducing the production of TXA₂ and consequently platelet aggregation¹². However, use of antiplatelets demands knowledge of their characteristics, risks and benefits, since they can cause severe adverse reaction as bleeding, neutropenia, thrombocytopenia and drug resistance^{13,14}.

Diarylisoaxazoles are well known COX-1 inhibitors¹⁵⁻¹⁸, abundantly studied also by X-ray in complex with the enzyme to gain insight of COX-1 catalytic core¹⁹. The selectivity towards COX-1 has advantages, such as inhibition of platelet TXA₂ production and lack of gastrointestinal toxicity^{20,21}, whereas non-selective COXs inhibitors have adverse cardiovascular side effects due

to their action as reducer of prostacyclin (PGI₂) biosynthesis, which has cardioprotective effect being a vasodilator and a potent platelet aggregation inhibitor^{22,23}. Herein, we report the design and synthesis of two sets of novel isoxazoles having the general formula mof-spacer-mof and mof-spacer-AA (Figure 1), respectively. They were evaluated as COXs and arachidonic acid-induced platelet aggregation inhibitors. *In vitro* coagulation, hemocompatibility to health human erythrocytes and cyto- and geno-toxicity tests were also performed. Structure Based Virtual Screening (SBVS) was carried out and the binding poses of selected compounds in the catalytic pockets of both COX-1 and COX-2 enzymes were analyzed²⁴.

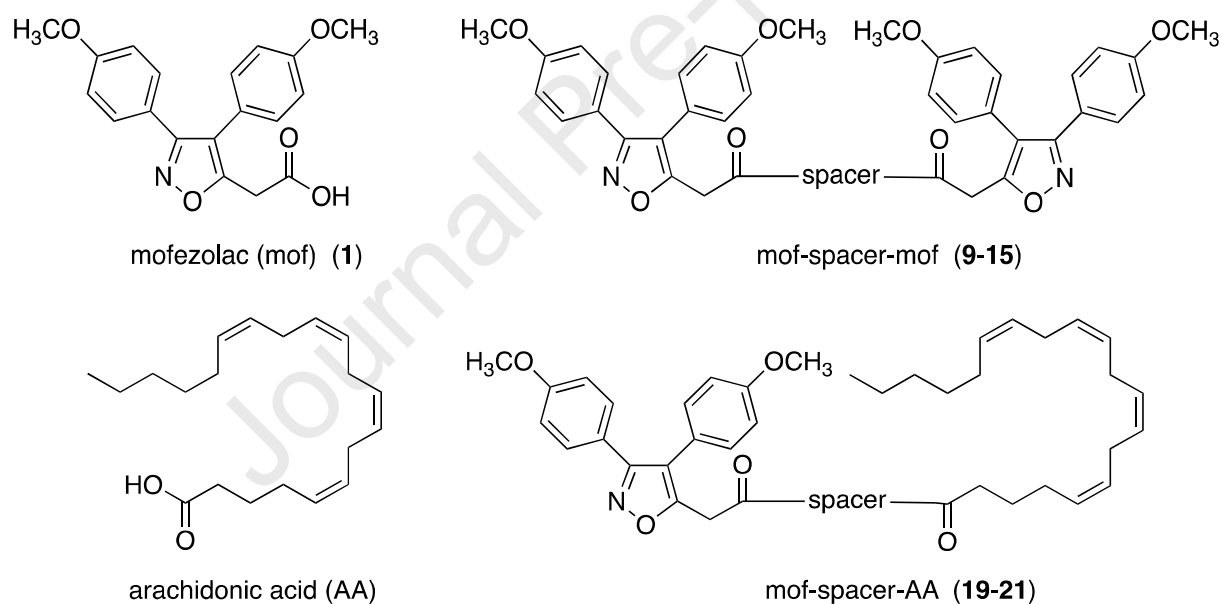


Figure 1. Chemical structures of mofezolac, arachidonic acid and two sets of novel isoxazoles (mofezolac-spacer-mofezolac and mofezolac-spacer-AA).

2. Results and discussion

COXs are homodimers composed of ~72 kDa subunits that are tightly bonded to one another via an interface spanning 2500 Å². Each COX monomer contains an epidermal growth factor-like domain, a membrane binding domain (MBD), and a large hydrophobic L-shaped catalytic core.

The bifunctional catalytic subunit houses both COX and peroxidase (POX) enzymatic activities. Both COX isoforms exhibit half-of-sites COX activity when a ligand binds to one monomer of an unoccupied dimer, that monomer becomes the allosteric subunit (Eallo), and the partner monomer becomes the catalytic monomer (Ecat). The catalytic efficiency of the catalytic monomer is determined by its interaction with its allosteric partner and this, in turn, is different for each different ligand that binds the allosteric monomer. With the aim to study the relationship between the activity of the two monomers, we have designed and prepared compounds bearing (i) two molecules of inhibitor linked by a spacer “**mofezolac-spacer-mofezolac**” (**mof-spacer-mof**) (**9-15**) or (ii) an inhibitor molecule linked to the arachidonic acid (COXs endogenous substrate) “**mofezolac-spacer-AA**” (**mof-spacer-AA**) (**19-21**) (Figure 1). Both two sets of molecules were projected with the idea that each compound eventually could simultaneously interact with the two monomers Eallo and Ecat, respectively, being formed by either two close mofezolac moieties or mofezolac and AA.

2.1 Rational behind the design of the novel compounds

The novel isoxazoles were though, as “double/hybrid molecules”, taking into consideration the dual characteristic of the COX-1 homodimer (PDB code 6Y3C) and the eventual cross-talk between monomers. The “double molecules” refers to compounds bearing two mofezolac units, instead “hybrid molecules” is used to indicate compound constituted by one mofezolac moiety and an arachidonic acid unit. Specifically, the novel molecules are constituted by two parts linked by a flexible or rigid moiety (spacer). One of the two parts is mofezolac (mof), a potent and selective COX-1 inhibitor (COX-1 $IC_{50} = 0.0079 \mu\text{M}$ and COX-2 $IC_{50} >50 \mu\text{M}$), mainly recognized by Arg120 residue located close to the COX membrane binding domain and at the

beginning of the long hydrophobic channel containing the COX catalytic site^{19,22} and the second molecular-part is another mofezolac molecule, affording mof-spacer-mof (double molecules **9-15**).

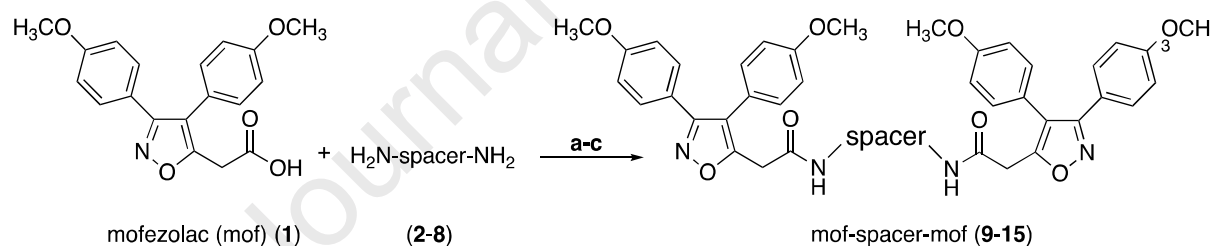
The hypothesis underlined such an overall structure is that the two monomers forming the COX homodimer play a different role, the first monomer when is occupied by a non-selective NSAIDs behaves as an allosteric enzymatic portion (Eallo), determining a conformational change of the partner monomer (Ecat) that exerts, then, the COX and POX catalysis. Hence, when one of the two mofezolac present in mof-spacer-mof interacts with Eallo, the second mofezolac should interact with Ecat, being close to it. This will definitively inhibit any COX catalytic activity.

The importance of understanding the cross-talk between the COX-allosteric and -catalytic monomers was highlighted by a work showing that COX-2 inhibitors can bind tightly to one monomer of COX-1 and attenuate the actions of aspirin on COX-1 *in vitro* and *in vivo*²⁵. From a pharmacological viewpoint, this condition resembles the case in which a patient treated with one of non-selective NSAIDs (i.e., a profen, such as ibuprofen) or COX-2 selective inhibitors (COXIBs: i.e., celeCOXib) to control an inflammatory status and contemporaneously takes the anti-platelet low-dose aspirin. In this case, it should be expected that ibuprofen binding to Eallo induces an Ecat conformational rearrangement to impair the aspirin access to Ecat catalytic site. This will favor, instead, the access of the arachidonic acid to Ecat. In other words, a patient that is treating inflammation with one of NSAIDs fails to prevent CVD events if simultaneously is assuming low-dose aspirin (85-300 mg/die targets only COX-1), because COX-1-Ecat is unoccupied and hence will still catalyze the conversion of AA in PGH₂, in turn transformed in thromboxane (TXA₂). Therefore, the “inflamed” patient believes to be protected against adverse CVD events but in practice he is not.

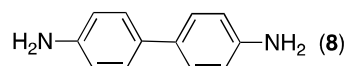
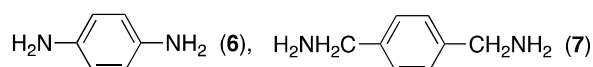
The second set of molecules “hybrid molecules”, were obtained by replacing one mofezolac unit with the arachidonic acid (AA), endogenous COX substrate, obtaining mof-spacer-AA compounds (**19-21**). In this case, the hypothesis is mof-moiety should interact with Eallo and AA moiety with Ecat.

2.2 Chemistry

For the preparation of the two acetamide bonds of "mof-spacer-mof" series (**9-15**), mofezolac was *in situ* activated in inert atmosphere with 1-(3-dimethylaminopropyl)-3-ethylcarbodiimide hydrochloride (EDC·HCl) and 1-hydroxybenzotriazole monohydrate (HOBt·H₂O) at 0 °C in anhydrous CH₂Cl₂ and then reacted with the opportune diamine (spacer) (**2-8**) in the presence of *N,N*-diisopropylethylamine (DIEA), affording, after overnight stirring the final products in 25-83 % yields (Scheme 1).

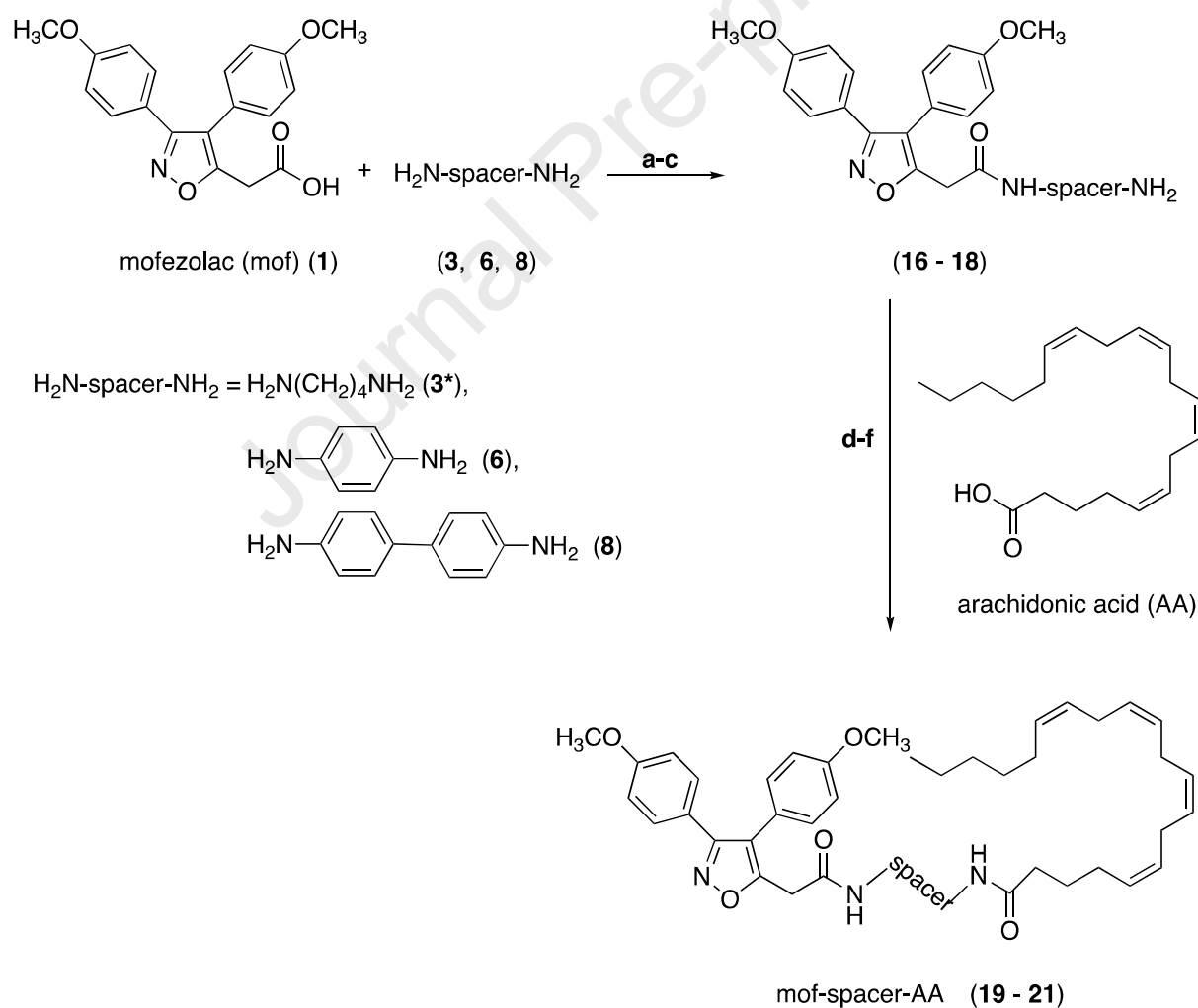


H₂N-spacer-NH₂ = H₂N(CH₂)₂NH₂ (**2**), H₂N(CH₂)₄NH₂ (**3**), H₂N(CH₂)₆NH₂ (**4**), H₂N(CH₂)₁₂NH₂ (**5**)



Scheme 1. Synthesis of mof-spacer-mof set (**9-15**). *Reagents and conditions:* (a) HOBt·H₂O, EDC·HCl, CH₂Cl₂, 0 °C, 2h; (b) diamine, DIEA, CH₂Cl₂, r.t., 16h; (c) H₂O.

With a similar approach the mofezolac/arachidonic bis-amides of mof-spacer-AA series were obtained by reacting mofezolac with the opportune diamine (1 mmol) (**3**, **6** and **8**), in the presence of *N,N*-diisopropylethylamine (DIEA), 1-hydroxybenzotriazole monohydrate (HOBt·H₂O) and 1-(3-dimethylaminopropyl)-3-ethylcarbodiimide hydrochloride (EDC·HCl) in anhydrous CH₂Cl₂ at 0 °C and under an inert atmosphere, affording the corresponding acetamides intermediates in 65-92 % yields (Scheme 2), that were finally reacted with arachidonic acid, activated by EDC·HCl and HOBt·H₂O, to afford the corresponding amides in 31-85 % yields.



Scheme 2. Synthesis of mof-spacer-NH₂ (**16-18**) and mof-spacer-AA (**19-21**). *Reagents and conditions:* (a) HOBt·H₂O, EDC·HCl, CH₂Cl₂, 0 °C, 2h; (b) H₂N-spacer-NH₂ (**3**, **6**, **8**; *1,4-diaminobutane (**3**) was first converted into NH₂(CH₂)₄NHBoc (**3a**) and allowed to react with mofezolac), DIEA, CH₂Cl₂, r.t., 16h; (c) H₂O; (d) **16-18**, DIEA, CH₂Cl₂, r.t.; (e) 2h stirred solution kept at 0 °C under argon of AA, HOBt·H₂O, EDC·HCl, CH₂Cl₂, r.t., 16h; (f) H₂O.

2.3 Cyclooxygenase catalytic activity inhibition evaluation

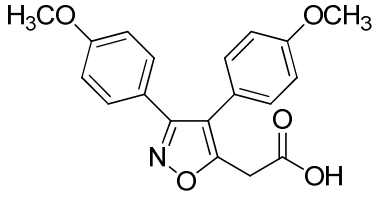
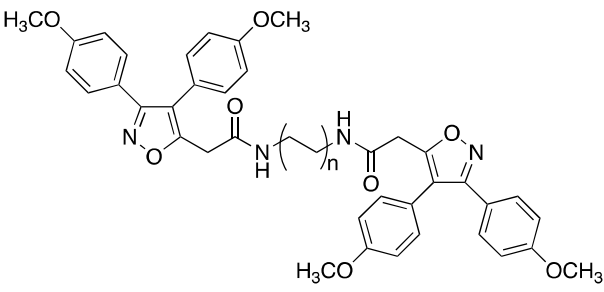
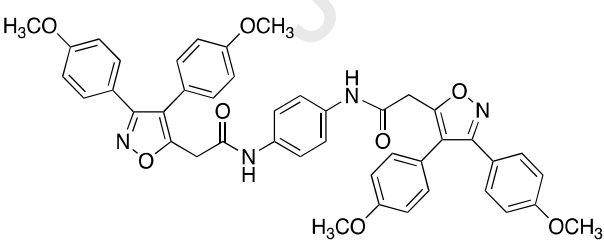
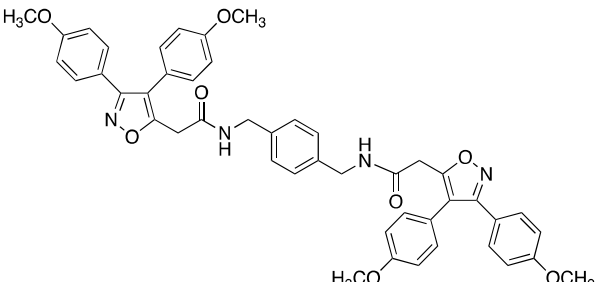
Cyclooxygenase activity inhibition was determined by a colorimetric COX Inhibitor Screening Assay which measures the peroxidase component (POX) of the cyclooxygenases, monitoring the appearance of oxidized *N, N, N', N'*-tetramethyl-*p*-phenylenediamine (TMPD) at $\lambda = 590$ nm (Table 1 and 2).

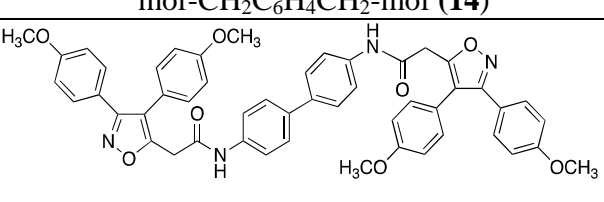
Mof-C₂-mof (**9**) is constituted by two mofezolac molecules linked by an ethylene bridge (Table 1). It inhibits both isoenzymes with a preference towards the COX-1 isoform (COX-1 IC₅₀ = 0.013 μ M and COX-2 IC₅₀ = 0.12 μ M), being its selectivity index SI equal to 9. A higher SI value is obtained by elongating the linker of two carbon units, substituting the ethylene to a butylene spacer, obtaining mof-C₄-mof (**10**). COX-1 selectivity is retained when the linker is longer, as in the case of mof-C₆-mof (**11**) and mof-C₁₂-mof (**12**), even if the inhibitory potency (IC₅₀) of COX-1 activity decreases (COX-1 IC₅₀ = 9.0 and 7.1 μ M, respectively). Mof-C₆H₄-mof (**13**) was obtained by replacing the C₂-C₁₂ carbon units as spacers by the conformationally rigid phenyl ring. A good grade of inhibition was restored registering an 85% percentage of inhibition, an IC₅₀ of 0.15 μ M and a SI of 333. No inhibition at all was observed towards both COX isoforms when a -CH₂C₆H₄CH₂- moiety was used as a spacer. The absence of any COXs activity inhibition by mof-CH₂C₆H₄CH₂-mof (**14**) was likely due to its higher possible conformational states. The presence of benzidine as a linker in mof-C₆H₄-mof (**13**) seemed to be responsible of its improved inhibitory activity with respect to **10-12**. This result prompted us to design the most selective compound of

the series (mof-C₆H₄-C₆H₄-mof) (**15**). Specifically, it has an IC₅₀ = 0.08 μM and an SI = 625 (Table 1).

Table 1. COX inhibitory activity of mof-spacer-mof molecules (**9-15**) bearing different spacers (**2-8**).

Journal Pre-proof

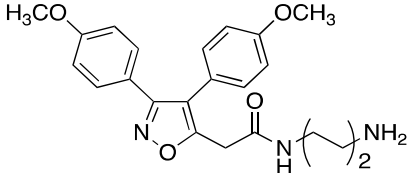
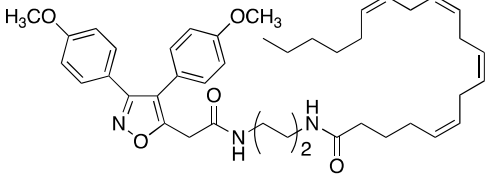
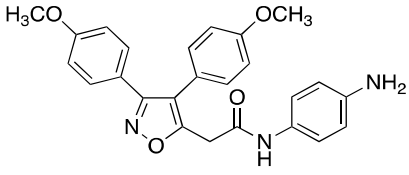
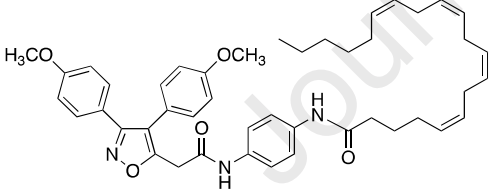
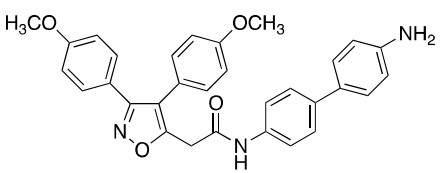
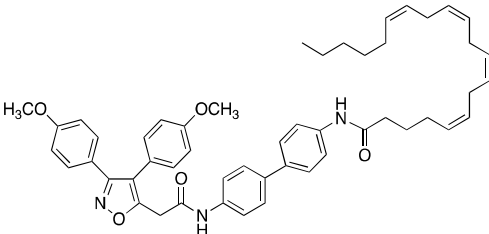
Compound	IC ₅₀ (μM) ^a (% inhibition) ^b		SI ^c	MW	cLogP ^e
	COX-1	COX-2			
 mofezolac (mof) (1)	0.0079 ± 0.15	>50	6392	339.11	2.51
 n = 1, spacer = -(CH ₂) ₂ - (mof-C ₂ -mof) (9)	0.013±0.0003 (75)	0.12±0.002 (45)	9	702.75	4.19
n = 2, spacer = -(CH ₂) ₄ - (mof-C ₄ -mof) (10)	5.5±0.1 (74)	>50	> 9	730.30	3.94
n = 3, spacer = -(CH ₂) ₆ - (mof-C ₆ -mof) (11)	9.0±0.2 (50)	>50	5.5	758.86	5.00
n = 6, spacer = -(CH ₂) ₁₂ - (mof-C ₁₂ -mof) (12)	7.1±0.3 (40)	>50	7	842.43	8.17
 mof-C ₆ H ₄ -mof (13)	0.15±0.04 (85)	>50	333	750.27	5.45
 mof-C ₁₂ H ₈ -mof (14)	>50 ^d	>50 ^d	-	778.30	5.49

mof-CH ₂ C ₆ H ₄ CH ₂ -mof (14)					
	0.08±0.001 (73)	>50	625	826.30	7.34
mof-C ₆ H ₄ -C ₆ H ₄ -mof (15)					

^aIC₅₀ values are the means of at least three independent measurements. ^bInhibition percentage (%) determined at the highest final inhibitor concentration used (50 μM). ^cSelectivity Index (SI) = COX-2 IC₅₀/COX-1 IC₅₀. ^eMeasured by using ChemBio3D Ultra.

Among the set of compounds mof-C₂÷C₁₂-mof (**9-12**) (Table 1), the alkyl C₄ spacer appeared to be the best length to achieve the highest COX-1 selectivity and a good extent of COX-1 activity inhibition. Then, the alkyl C₄ spacer was used to conjugate mofezolac to arachidonic acid (AA) (Scheme 2, Table 2), the natural endogenous COXs substrate. In this case, an inversion of selectivity was observed. In fact, mof-C₄-AA (**19**) is a preferential COX-2 inhibitor with a COX-2 IC₅₀ of 0.8 μM, even though its precursor mof-C₄-NH₂ (**16**) is a COX-1 selective inhibitor (COX-1 IC₅₀ = 0.95 μM, COX-2 IC₅₀ = 3.5 μM). As from Table 1, COX-1 inhibition preference was observed when a phenyl ring is the spacer in mof-C₆H₄-mof (**13**). The corresponding mof-C₆H₄-AA (**20**) was found to be the most potent and selective COX-1 inhibitor of the series with a COX-1 IC₅₀ of 0.05 μM, COX-2 IC₅₀ > 50 μM, and a selectivity index higher than 1,000. Its precursor mof-C₆H₄-NH₂ (**17**), instead, exhibited a COX-2 inhibition preference (COX-1 IC₅₀ = 24.0 μM, COX-2 IC₅₀ = 0.5 μM). The COXs selectivity preference in favor of COX-2 (SI = 189) was also observed when a benzidine was used as spacer to prepare mof-C₆H₄-C₆H₄-AA (**21**). Such a SI value is higher than any of COXIBs selectivity, despite of the behavior of its precursor (**18**) that showed a COX-1 inhibition preference (COX-1 IC₅₀ = 0.075 μM, COX-2 IC₅₀ = 0.3 μM).

Table 2. COX inhibitory activity of compounds composed by mofezolac and arachidonic acid (**19-21**) and their precursors (mofezolac linked to the spacers) (**16-18**).

Compound	IC ₅₀ (μM) ^a (% inhibition) ^b		SI ^c (1/SI)	MW	cLogP ^d
	COX-1	COX-2			
 mof-C ₄ -NH ₂ (16)	0.95±0.01 (100)	3.5±0.12 (51)	3.7 (0.27)	409.20	1.49
 mof-C ₄ -AA (19)	16.0±0.2 (57)	0.8±0.02 (61)	0.05 (20)	695.43	8.66
 mof-C ₆ H ₄ -NH ₂ (17)	24.0±0.9 (74)	0.5±0.0 (79)	0.02 (48)	429.17	2.57
 mof-C ₆ H ₄ -AA (20)	0.05±0.002 (66)	>50	> 1,000 (> 0.001)	715.40	10.44
 mof-C ₆ H ₄ -C ₆ H ₄ -NH ₂ (18)	0.075±0.002 (85)	0.3±0.01 (71)	4 (0.25)	505.20	4.46
 mof-C ₆ H ₄ -AA (20)	17±0.7 (50)	0.09±0.003 (60)	0.005 (189)	791.43	12.29

mof-C ₆ H ₄ -C ₆ H ₄ -AA (21)					
------------------------------------------------------------------------------------	--	--	--	--	--

^aIC₅₀ values are the means of at least three independent measurements. ^bInhibition percentage (%) determined at the highest final inhibitor concentration used (50 μM). ^cSelectivity Index (SI) = COX-2 IC₅₀/COX-1 IC₅₀. ^dMeasured by using ChemBio3D Ultra.

It is evident from the data listed in Table 1 and 2, that even if more and more work has been done to understand the rationale behind the selectivity of COXs inhibitors no definitive rules are available to design a highly selective COX-1 or COX-2 inhibitor. The two sets of the novel mof-spacer-mof and mof-spacer-AA were projected to try to define the role of Eallo and Ecat, the two monomers forming the COX homodimers, often considered conformationally heterodimers²⁵. The condition used to measure the inhibitory capability of the novel compounds requires an arachidonic acid concentration kept at 100 μM. The highest concentration at which the new sets of compounds are usually tested is 50 μM, this could mean that if AA has a higher affinity for Eallo (0.25 μM for both COX isoforms) than for Ecat (0.5-2.0 and 5.0-10.0 μM for COX-1 and COX-2, respectively) there could be both a AA mass effect along and compounds chemical structures (size, polarity, lipo- and hydro-philia, the presence of specific functional groups, specific interactions with the almost 50 amino acid interactions present in the long hydrophobic channel constituting the COXs active site and involved in the substrate/inhibitors recognition) to direct the selectivity of inhibitors either towards COX-1 or COX-2. *In vivo*, the situation is still more complex for the presence of circulating saturated, mono- and poly-unsaturated fatty acids. Saturated and mono-unsaturated free fatty acids bind Eallo, act as COXs non-substrates, and when their ratio with respect AA is equal or higher than 20, they behave as inhibitors of COX-1 and activator of COX-2. Poly-unsaturated fatty acids bind Ecat of COX-1 but Eallo of COX-2 and this could be the reason of the cardioprotective role of ω-3 fish oil fatty acids, particularly when ω-3 fatty acids/AA ratios are equal or higher than 5.0.

2.4 Molecular Modeling

A Structure Based Virtual Screening (SBVS), based on the Fingerprints for Ligands and Proteins (FLAP) algorithm, was carried out as an attempt to rationalize the inhibition capabilities of the novel synthesized compounds and the binding poses of selected compounds in the catalytic pockets of both COX-1 and COX-2 enzymes were analyzed¹⁹.

The SBVS was performed using the X-ray crystal structures of ovine COX-1 in complex with mofezolac (PDB code: 5WBE)¹⁹ or AA (PDB code: 1DIY)²⁶ and of mouse COX-2 with celeCOXib (PDB code: 3LN1)²⁷, upon removal of the co-crystallized ligands. The COX-1 binding poses of the mof-spacer-mof compounds (**9**, **13** and **15**) were generated within the internal cavities computed for the 5WBE structure; both COX-1 structures (5WBE and 1DIY) were used to investigate the mof-spacer-AA compounds (**19**, **20** and **21**) and, interestingly, similar binding poses were obtained. As in our previous studies^{28,29}, the crystallographic poses of mofezolac¹⁹ and celeCOXib²⁷ in the three-dimensional structure of COX-1 and COX-2, respectively, as well as that of AA in COX-1²⁶, were also reported for comparison purposes (Figure S1-S3).

According to the FLAP poses of the mof-spacer-mof compounds (**9**, **13** and **15**) within COX-1 (Figure 2), one of the two mofezolac moieties is always located at the top of the catalytic pocket. The insertion of different flexible or rigid spacers induced significant changes in the interactions of both the inner and the outermost mofezolac units. Overall, these compounds strongly interact with (i) the residues Arg120/Tyr355 at the catalytic site entry channel, an enzyme zone crucial for substrate/inhibitor recognition, (ii) the residues in the central hydrophobic region and (iii) the top of the cavity, where the catalytic inducer Tyr385 is located.

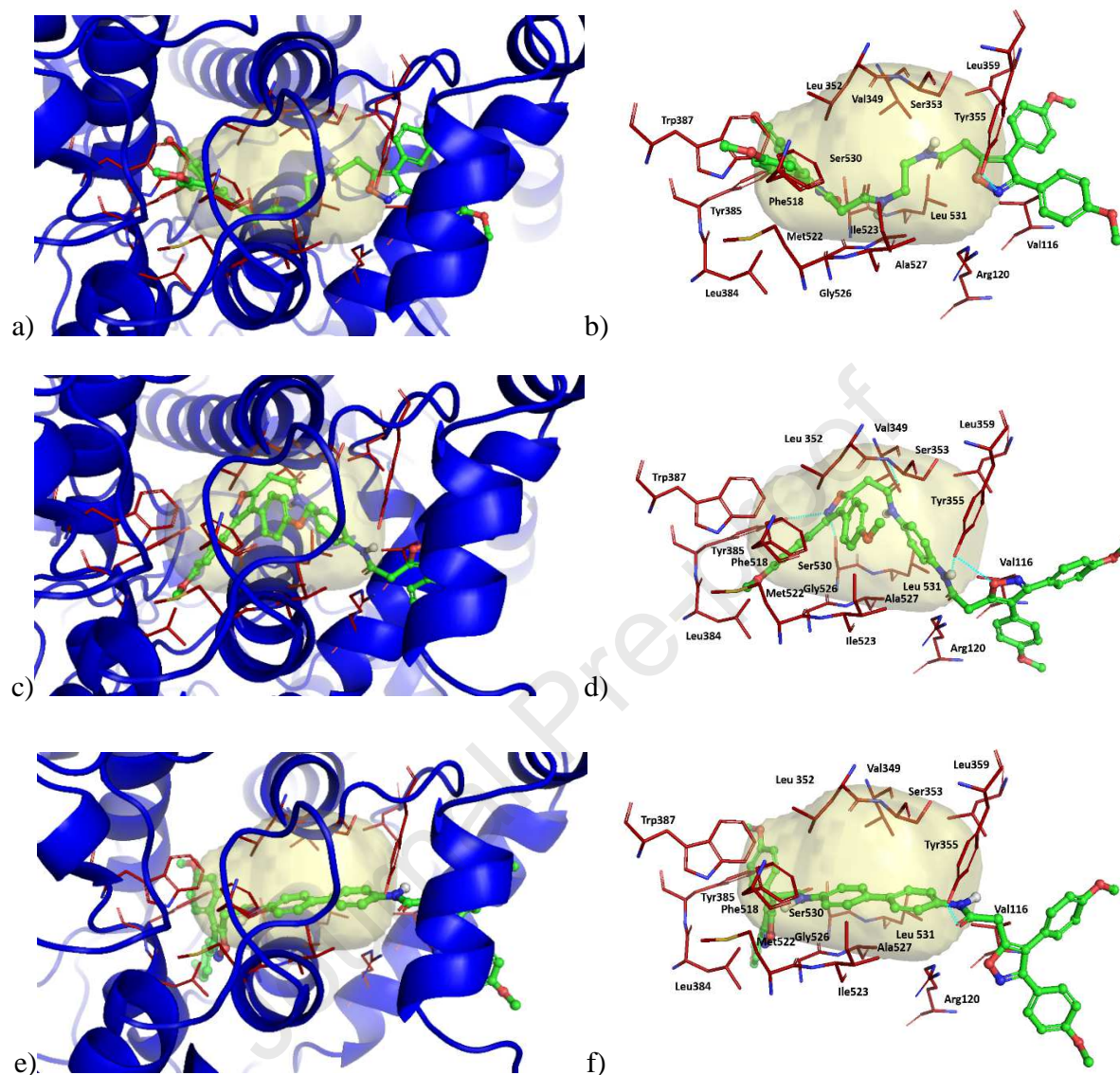


Figure 2. Proposed 3D binding mode inside the active site of COX-1, determined by FLAP analysis, for **9** (a, b), **13** (c, d) and **15** (e, f). Some of the COX-1 key residues located in the cavity are highlighted in stick-mode.

The key hydrogen bond with Tyr355 occurred for all compounds, even though the H-bond acceptor is the isoxazole nitrogen atom of the outer mofezolac for **9**, the outer amide (NH) and the isoxazole ring are the donor and acceptor unit, respectively, for **13** and only the amide carbonyl (CO) for **15**. The methoxy substituted phenyl ring of the outer mofezolac moieties (Figure S4) interacts with an external region defined by two parallel α -helices (one of the two helices

containing also the Arg120). Hydrophobic and H-bond interactions (with the Tyr385), of both the mofezolac inner moiety and the spacer moieties, inside the cavity contributed to obtain a favorable binding for all the compounds.

A good fit inside the catalytic cavity and H-bond acceptor interactions, quantified by the FLAP H and O probes respectively, relate to the compounds ability to act as COX-1 inhibitors. The analysis of these parameters, in agreement with experimental data (Table 1), confirms that compound **9** is the most active of the series while compounds **13** and **15** are almost equivalent (H^*O values are 0.62, 0.56, and 0.58, respectively), albeit with lower values than the reference inhibitor mofezolac, whose H^*O value is 0.70.

A deeper inspection of the binding poses (2D depiction in Figure 3 and Figure S5), allowed to ascertain that the compound **9**, bearing the flexible and shorter C_2 unit spacer, displays the most efficient interactions with both Arg120 and Tyr355 (Figure 3a); the biphenyl unit of **15** ensures the best interaction with the central hydrophobic region defined by the residues of the two parallel α -helixes that define the upper and the lower limits of the catalytic cavity (Figure 3b). In addition, the external mofezolac unit of **15** is able to form a dense network of CH- π interactions between the methoxy-substituted phenyl rings and different Val, Leu and Ile residues of the two-parallel outermost α -helixes (Figure S4c). On the contrary, in the FLAP binding pose of **13**, the inner mofezolac moiety shifts towards the center of the cavity (Figure S5); this shift allows the formation of a new H-bond interaction between Tyr355 and amide NH, but the outer mofezolac is involved in less efficient CH- π interactions. Additional π - π interaction with Phe518, or other aromatic residues, and H-bond are still possible for all the compounds.

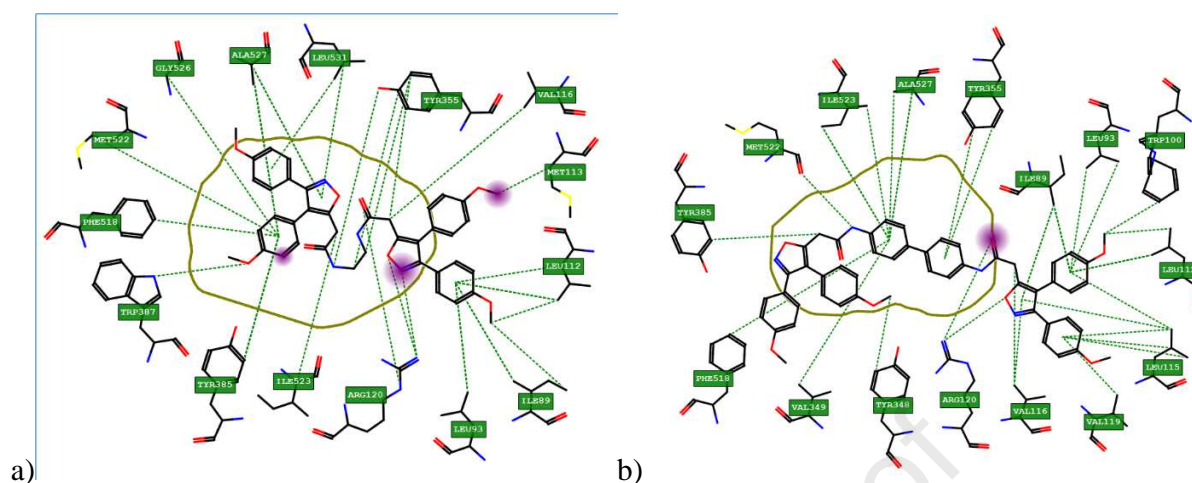
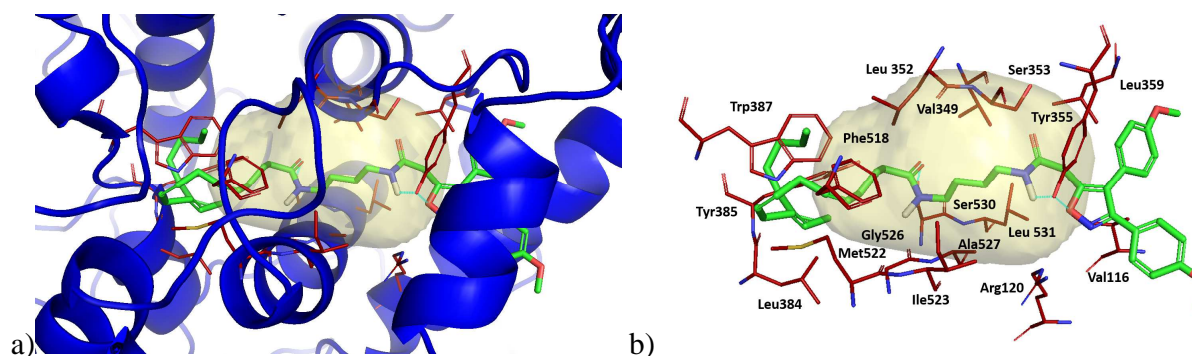


Figure 3. Comparison of the 2D FLAP binding poses for **9** (a) vs **15** (b). The most important COX-1 residues are shown together with their respective numbers. Purple regions indicate strong interactions.

The FLAP poses of the ‘hybrid molecules’ **19**, **20** and **21** within the COX-1 show that they interact with the catalytic cavity through the fatty acid moiety (Figure 4), while the mofezolac is always located in the outer region of the COX-1 active site. The features of the spacer linking the mofezolac and AA, also in this series, guide the interactions established within the catalytic site, resulting, then, in the enzyme activity inhibition.



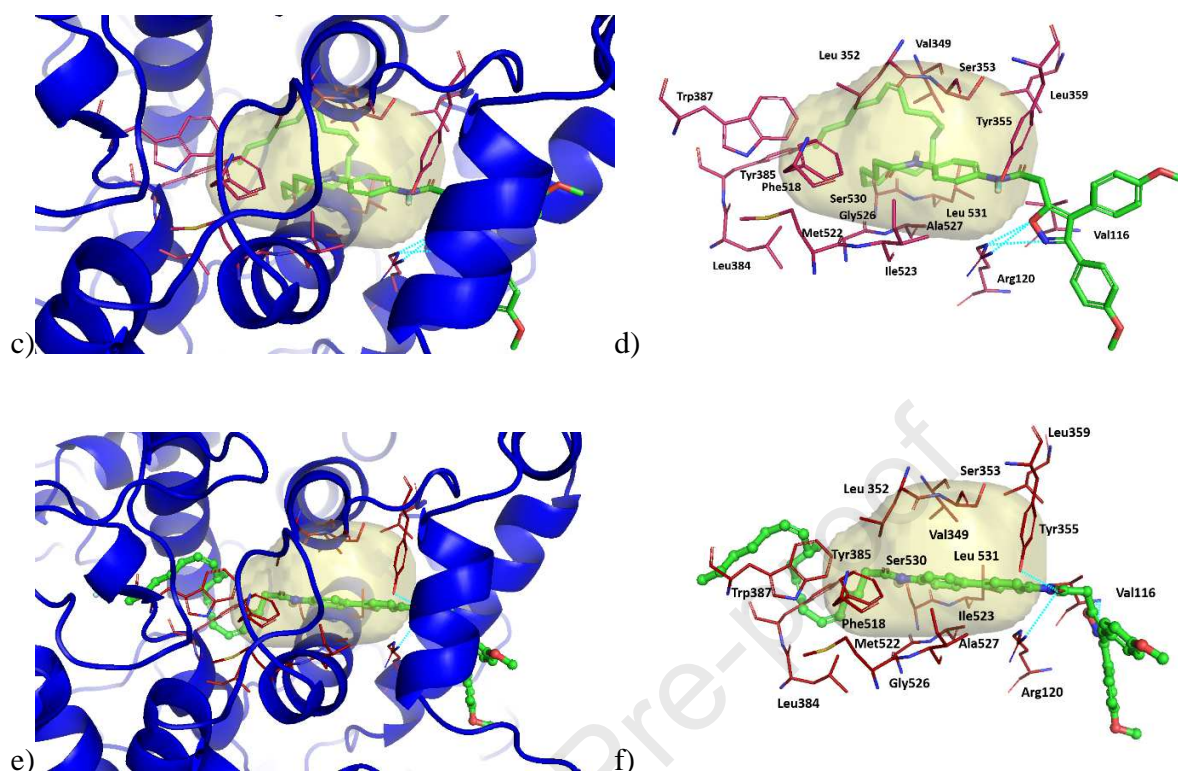


Figure 4. Proposed 3D binding mode inside the active site of COX-1, determined from FLAP analysis, for **19** (a, b), **20** (c, d) and **21** (e, f). Some of the COX-1 key residues located in the cavity are highlighted in stick-mode.

Only compound **20** is able to realize (i) a good fit of the long AA chain inside the catalytic cavity, (ii) strong H-bond interactions with Arg120 and Tyr355, and (iii) efficient interactions both with the central hydrophobic area of the cavity and with the aromatic residues in the deepest region, i.e. nearby the catalytic Tyr385 (Figure 5; the poses of **19** and **21** are shown for comparison in Figure S6). It is possible to take advantage of the CH- π interactions between the central phenyl ring and the residues of the two parallel α -helices and, at the same time, to establish strong H-bond with the outer amide linkage and the mofezolac-isoxazole. Moreover, as previously reported for **9** and **15**, the methoxy-substituted phenyl rings of the mofezolac unit realize a dense network of CH- π interactions with the Val, Leu and Ile residues of the two-parallel outermost α -helices.

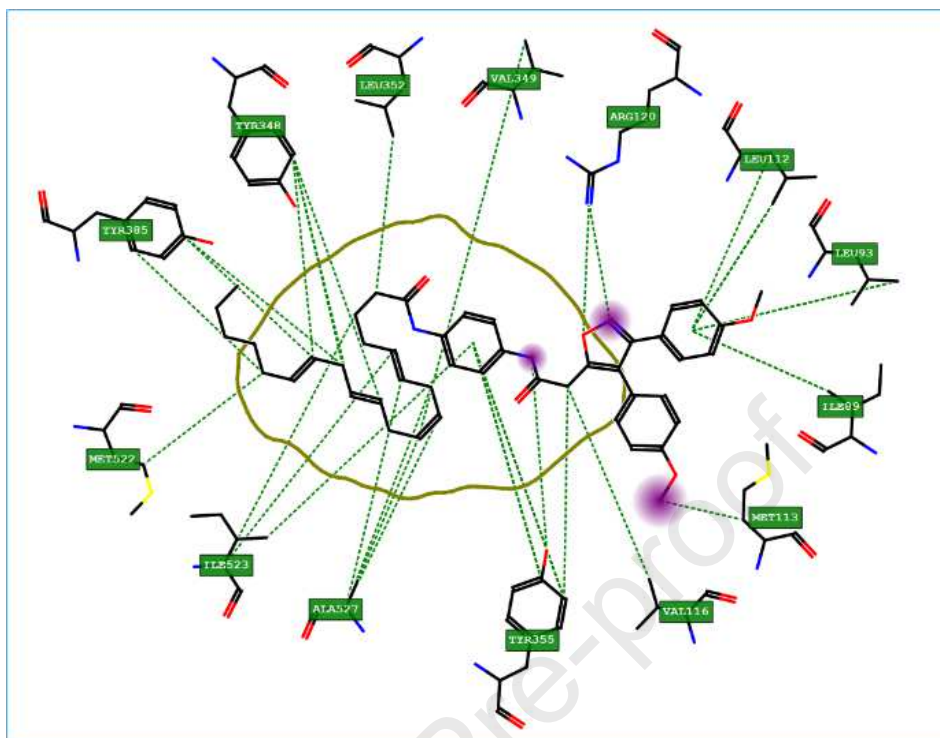


Figure 5. 2D FLAP binding pose of compound **20**. The most important COX-1 residues are shown together with their respective numbers. Purple regions indicate strong interactions.

A check of the FLAP H and O probes, which correlated with the *in vitro* inhibitor behavior, allowed us to rationalize that **20** is the most active of the series: the H*O values obtained through the Structure Based Virtual Screening are 0.52, 0.50, and 0.47 for **20**, **19** and **21**, respectively.

It is worth noting that, when the AA moiety is removed (i.e. compounds **16**, **17** and **18**) the trend observed for the inhibitory activity reverses and resembles what previously observed for ‘gemini systems’ **9**, **13** and **15**, when one of the mofezolac and the spacer occupy the enzyme cavity. This result further supports the inclusion of the substrate/AA moiety and the lower inhibition potency observed for **19** and **21** than **20**.

Among the synthesized compounds, only **9**, **19** and **21** inhibit COX-2; although the mofezolac is not a COX-2 inhibitor, the FLAP binding poses clearly indicate that this moiety is always included, at variable depths, into the wider COX-2 cavity (Figure 6).

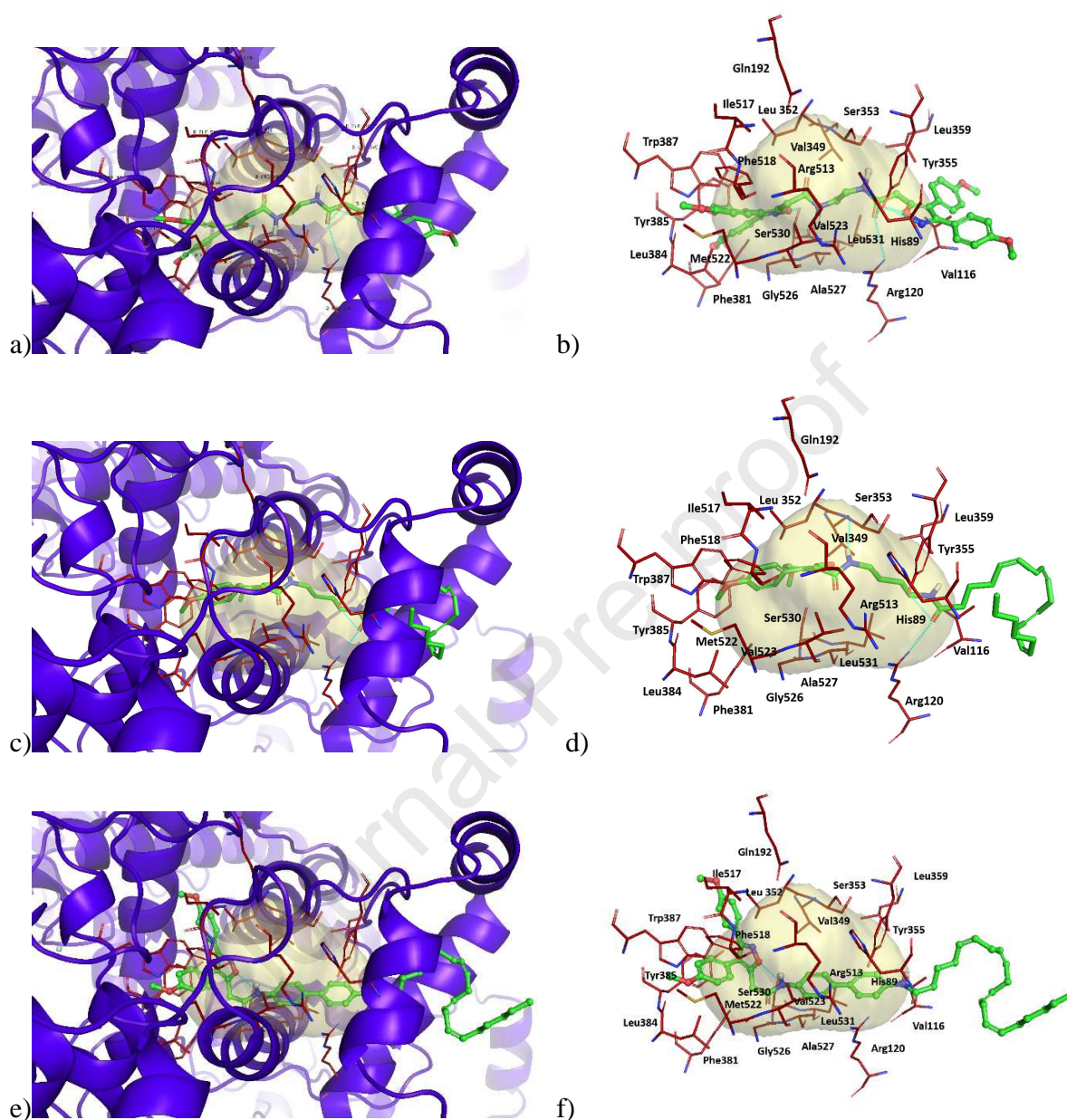


Figure 6. Proposed 3D binding mode inside the COX-2 active site determined by FLAP analysis for **9** (a, b), **19** (c, d) and **21** (e, f). Some of the COX-1 key residues located in the cavity are highlighted in stick-mode.

The compounds with the short and flexible spacer, namely **9** and **19**, place the mofezolac unit at the bottom of the cavity mainly due to a network of CH- π , S- π and π - π interactions (Figure 6 and 7) and the H-bond interaction of the isoxazole ring with Ser530. Some of these interactions can be

observed also in the crystallographic pose of celeCOXib (Figure S3). An additional network of H-bonds, between Arg120/Tyr355 and both the amidic carbonyl (CO) and the outer isoxazole ring, and CH- π interaction, of the external mofezolac, at the entry of the cavity reinforces the overall interaction of compound **9** with the enzyme. For compound **19**, only the amidic carbonyl (CO) is hydrogen-bonded to Tyr355; moreover, the AA moiety (Figures 6c, 6d and S8) is too close to the two-parallel outermost α -helixes that define the cavity entry causing steric hindrance.

The FLAP binding pose of **21** inside the COX-2 catalytic site (Figure 6e, 6f and 7) shows that mofezolac has a different orientation but is able to achieve strong π - π and S- π interactions, with Met 522 and Tyr 385; the latter residue and Ser 530 are involved in H-bond interactions with the isoxazole ring and the inner amidic NH; the biphenyl unit is located in the central region of the binding pocket and interact with Tyr355 and the residues that define the upper and lower cavity walls. Unlike compound **9** and **19**, the AA moiety of **21** establishes strong CH- π interaction with the external parallel α -helixes and strong H-bond with Arg120: these interactions are key points for the inhibitory activity of this compound (Figure S9-11).

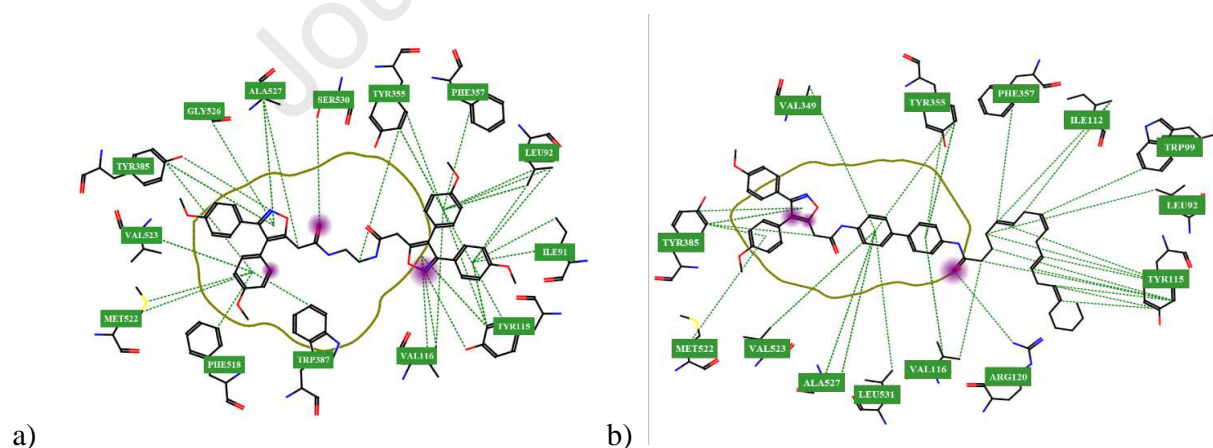


Figure 7. Comparison of the 2D FLAP binding poses for compounds **9** (a) vs **21** (b). The most important COX-2 residues are shown together with their respective numbers. Purple regions indicate strong interactions.

Hydrophobic interaction and H-bond acceptor interactions, quantified by the FLAP probes Dry and O respectively, are strictly related to the COX-2 inhibition activity; the analysis of these parameters confirms that **19** is the less active of the series, whereas compounds **9** and **21** are almost equivalent (Dry*O values are 0.70 and 0.77, respectively) (Figure 7).

The Structure Based Virtual Screening clearly indicates that small structural differences lead to large variations in the inhibition activity, not only towards the single COX isoform but also when comparing the activity of the same substrate towards the two COX isoforms. This is not surprising as the different catalytic activity and substrate selectivity of COX-1 and COX-2 are determined by a single amino acid difference in the active site (valine 509 to isoleucine) and a series of differences at the entry channel of the active site²⁸.

Steric effects, hydrophobic contacts (evaluated by the probe H, Dry and O) and H-bond acceptor sites of the compounds with the enzyme key regions help us to clarify the inhibition activity observed. For example, the biphenyl spacer in compound **15** shows good potency towards COX-1, but is not tolerated in the hybrid inhibitor **21**; the selectivity is reversed when considering the inhibition activity towards COX-2. The inhibition activity of **15** towards COX-1 is mainly determined by interaction within the smaller cavity and at the catalytic site entry channel; it is not possible to define a comparable interaction towards the COX-2 isoform as the small mofezolac unit inside does not realize a good fit with the key region of the catalytic cavity while the outer mofezolac unit experiences large steric hindrance with the extended entry mouth.

Hybrid molecules **19-21** are able to inhibit both COX isoforms but the overall effect derives from different interaction: the arachidonic acid moiety is always included in the cavity of the COX-1 while the mofezolac unit occupies the COX-2 catalytic site. The phenyl moiety in compound **20** ensures the right complementarity (shape and interaction), then the highest inhibition, towards COX-1. Only the biphenyl spacer of compound **21** allows effective interactions with the catalytic

site and the mouth of the cavity for the COX-2 isoform, at the same time the interaction of the arachidonic acid with enzyme entry channel operates in a synergic way; taken together, these effects determine the reversed selectivity.

Compounds **13**, **15**, **20-21** were further characterized by evaluating their contribution in platelet aggregation and blood coagulation and their hemolytic and genotoxicity effects as a continuation of preceding investigations, mofezolac and its analogues have already been described as an attempt to target diseases such as multiple myeloma²⁹⁻³¹, thrombosis³², and ovarian cancer³³⁻³⁵.

2.5 Inhibition of AA-induced Platelet aggregation

The IC₅₀ values (Table 3) show that all compounds were able to efficiently inhibit platelet aggregation. In particular, mof-C₆H₄-C₆H₄-mof (**15**) shows an IC₅₀ = 0.44 μM superimposed with mofezolac (IC₅₀ = 0.45 μM). All other compounds **13**, **2** and **20** have a comparable micromolar activity revealing the potency of these antiplatelet compounds to inhibit the arachidonic acid pathway of platelet aggregation and confirm their ability to reduce the TXA₂ production by COX-1 inhibition as a mechanism to impair normal platelet aggregation as for aspirin (IC₅₀ = 1.11 μM)³¹.

Table 3. Antiplatelet profile of compounds on *in vitro* platelet aggregation of human citrated platelet rich plasma induced by arachidonic acid (AA).

Compound	IC ₅₀ (μM) ^a
mof-C ₆ H ₄ -mof (13)	0.91 ± 0.28
mof-C ₆ H ₄ -C ₆ H ₄ -mof (15)	0.44 ± 0.13
mof-C ₆ H ₄ -AA (20)	0.61 ± 0.24
mof-C ₆ H ₄ -C ₆ H ₄ -AA (21)	0.76 ± 0.16
mofezolac (1)	0.45 ± 0.04
Aspirin	1.11 ± 1.17

^aIC₅₀ = concentration at which 50% inhibition of platelet aggregation is observed.

2.6 *In vitro* coagulation assays

Neither the extrinsic nor intrinsic pathways of the coagulation cascade were affected by the presence of the novel isoxazoles, suggesting that their antithrombotic profile relies on the direct impairment of platelet aggregation, thus differing from dual action molecules (Table 4). This result reveals a small bleeding risk in comparison to dual acting molecules whose mechanism often leads to severe bleeding disorders³⁶.

Table 4. *In vitro* coagulation of human plasma (n = 3) activated by prothrombin time (PT) and thromboplastin time (APTT).^a

Compound (100μM)	PT (seconds)	APTT (seconds)
C -	13.9 ± 0.8	44.8 ± 1.5
C +	300 ± 0.0	300 ± 0.0
mof-C ₆ H ₄ -mof (13)	15.5 ± 0.0	47.5 ± 0.4
mof-C ₆ H ₄ -C ₆ H ₄ -mof (15)	15.1 ± 0.3	46.5 ± 1.1
mof-C ₆ H ₄ -AA (20)	15.3 ± 1.0	55.6 ± 1.2
mof-C ₆ H ₄ -C ₆ H ₄ -AA (21)	14.6 ± 0.5	48.0 ± 1.6
mofezolac (1)	14.2 ± 0.3	50.8 ± 0.23
Aspirin	14.6 ± 1.0	50.3 ± 0.3

^a(C-) = negative control: DMSO 1%. (C+) = positive control: 100 μM rivaroxaban.

2.7 Hemocompatibility to healthy human erythrocytes

The hemocompatibility profile of some representative novel isoxazoles was determined based on the degree of erythrocyte lysis observed in the 3h incubation time at 37°C. The hemolysis values

obtained were zero (%) or close to it, confirming the acceptable toxicity profile of the compounds tested (Table 5). Hemolysis values below 10% are considered non-hemolytic³⁷.

Table 5. Hemolytic profile of some representative novel isoxazoles through hemolysis assay.^a

Compound (100 μ M)	Hemolysis (%)
C-	0.00 \pm 0.22
C+	100 \pm 2.01
mof-C ₆ H ₄ -mof (13)	0.00 \pm 0.04
mof-C ₆ H ₄ -C ₆ H ₄ -mof (15)	0.00 \pm 0.08
mof-C ₆ H ₄ -AA (20)	0.00 \pm 0.01
mof-C ₆ H ₄ -C ₆ H ₄ -AA (21)	0.14 \pm 0.08
mofezolac (1)	0.00 \pm 0.02
Aspirin	0.0 \pm 0.04

^a(C-) = 1% DMSO is the negative control; 1% Triton X-100 is the positive control (C+). Values below 10% are considered non hemolytic.

2.8 Cytotoxicity activity

The cytotoxicity test in Vero cell line was performed by MTT reduction assay at 10 and 100 μ M for 48 hours (Table 6). Among all the tested compounds, none of them was considered toxic to Vero cells, even at higher concentrations. Significantly statistical reduction (p-value \leq 0.05) of cell viability values was not considered in this test, since the results above 70% are biologically acceptable according to ISO 10993:5 (2009). This result represents a starting point for advanced pre-clinical studies, given the correlation between toxicity in Vero cells, isolated renal tissue and nephrotoxicity in rats³⁸.

Table 6. Vero cells viability after 48 hours of exposition to the tested novel compounds at 10 and 100 μ M.^a

Compounds	[μ M]	Cell viability (%)	\pm S.D. (%)
Control	-	100	2.6
mof-C ₆ H ₄ -mof (13)	100	97	2.8
	10	98	0.5
mof-C ₆ H ₄ -C ₆ H ₄ -mof (15)	100	92	2.8
	10	100	4.8
mof-C ₆ H ₄ -AA (20)	100	79	3.2
	10	93	2.8
mof-C ₆ H ₄ -C ₆ H ₄ -AA (21)	100	84	3.1
	10	94	4.2
mofezolac (1)	100	91	4.6
	10	97	3.7
Aspirin	100	95	2.0
	10	100	2.8

^aData are presented as mean of cell viability values (n = 4) \pm standard deviations.

2.9 Genotoxicity Tests

The safety of the novel isoxazoles is reinforced by the genotoxicity tests which revealed no mutagenicity profile against *Salmonella typhimurium* auxotroph mutant strains through reverse mutagenesis and histidine prototrophy (Ames test), compared to the positive control 4-nitroquinoline 1-oxide (4NQO), nor genotoxicity evaluated against *Escherichia coli* through the SOS chromotest. This low risk profile is observed even at the highest concentrations tested (500 μ M, Table 7), revealing the safety profile of the series as promising “lead prototypes”.

Table 7. Mutagenic and genotoxic activity of molecules without metabolic activation.^a

	Ames Test	SOS chromotest
--	-----------	----------------

Compound	<i>S. typhimurium</i>				<i>E. coli</i>	
	TA97	TA98	TA100	TA102	PQ35	PQ37
mof-C ₆ H ₄ -mof (13)	-	-	-	-	-	-
mof-C ₆ H ₄ -C ₆ H ₄ -mof (15)	-	-	-	-	-	-
mof-C ₆ H ₄ -AA (20)	-	-	-	-	-	-
mof- C ₆ H ₄ -C ₆ H ₄ -AA (21)	-	-	-	-	-	-
mofezolac (1)	-	-	-	-	-	-
4-NQO	+	+	+	+	+	+
DMSO	-	-	-	-	-	-
Aspirin	-	-	-	-	-	-

^aAssays performed by dissolving the tested compounds in DMSO. 4-NQO was used as a positive control. Reported results derive by three different concentrations (10 μ M, 100 μ M and 500 μ M).

3. Conclusion

New double/hybrid molecules (mof-spacer-mof/mof-spacer-AA) have been investigated for their cross-talk between the E_{allo} and E_{cat} monomers constituting the COX structure. Molecular modeling accomplished studies clearly show the importance of the novel compounds interaction not only inside the catalytic cavity but also at the entry channel, thus supporting the extreme importance of allosteric effects in the COX catalytic activity. Depending on the nature of the spacer linking the two moieties (two mofezolac molecules or mofezolac bond to arachidonic acid) of the novel compounds resulted to have a different inhibition preference towards COX isoforms but all of them were endowed with antiplatelet activity. In addition, these compounds were not able to affect the coagulation pathways, showing selectivity for primary hemostasis related targets. The hemolysis values were below 10 % indicating a non-hemolytic profile of such compounds. Their safety profile was proven also by both cytotoxicity activity and genotoxicity tests. Thus, the

novel compounds have shown a good pharmacodynamic profile and selectivity in COX-1 or COX-2 inhibition, revealing that they might be promising antiplatelet agents. Further studies are ongoing to produce some crystallographic structure of the human COX isoenzymes taking also into account the recent publication of the long-sought 3D structure of human COX-1 (PDB code: 6Y3C) in the Protein Data Bank.

4. EXPERIMENTAL SECTION

Chemistry. ^1H NMR and ^{13}C NMR spectra were recorded on a Bruker 600 MHz or AGILENT 500 MHz spectrometer and chemical shifts are reported in parts per million (δ), and the following abbreviations were used to explain the multiplicities: s = singlet, d = doublet, t = triplet, q = quartet, m = multiplet, quin = quintuplet, sext = sextet, sep = septet, b = broad. FT-IR spectra were recorded on a Perkin-Elmer 681 spectrophotometer. GC analyses were performed on a HP 6890 model, Series II by using a HP1 column (methyl siloxane; 30 m x 0.32 mm x 0.25 μm film thickness). Analytical thin-layer chromatography (TLC) was carried out on pre-coated 0.25 mm thick plates of Kieselgel 60 F254; visualization was accomplished by UV light (254 nm). Column chromatography was accomplished by using silica gel 60 with a particle size distribution 40–63 μm and 230-400 ASTM. GC-MS analyses were performed on HP 5995C model. High-resolution mass spectrometry (HRMS) analyses were performed using a Bruker microTOF QII mass spectrometer equipped with an electrospray ion source (ESI). Reagents and solvents were purchased from Sigma-Aldrich (Sigma-Aldrich, St. Louis, MO, USA) and used without any further purification. Full characterization data have been reported for both the newly synthesized compounds and the known compounds. All spectral data are consistent with the reported values.

General procedure for the preparation of mofezolac-spacer-mofezolac (9-15). To a solution of mofezolac (3 mmol) in anhydrous CH_2Cl_2 kept at 0°C in an argon-flushed three-necked round

bottom flask, equipped with a magnetic stirrer and an argon inlet, 1-hydroxybenzotriazole monohydrate (HOBt·H₂O, 3 mmol) and 1-(3-dimethylaminopropyl)-3-ethylcarbodiimide hydrochloride (EDC·HCl, 3 mmol) were added. The yellow and limpid reaction mixture was stirred for 2h at 0 °C. Then, the proper diamine (**2-8**, 1 mmol) and *N,N*-diisopropylethylamine (DIEA, 3 mmol) were very slowly added by a syringe, and the mixture stirred overnight (16h) kept under argon atmosphere. The reaction was blocked by adding H₂O and extracted by EtOAc (3 x 15 mL). The combined organic extracts were washed with sat. NaHCO₃ (3 x 5 mL), dried with anhydrous Na₂SO₄, filtered and the solvent removed under reduced pressure. The solid reaction crudes were purified by crystallization from EtOAc/hexane mixtures.

***N,N'*-(Ethane-1,2-di-yl)-bis{2-[3,4-bis(4-methoxyphenyl)isoxazol-5-yl]acetamide}** (**9**). 27% Yield. Mp 145-148 °C (EtOAc/Hexane, white solid). FT-IR (KBr): 3852, 3741, 2959, 2915, 1638, 1380, 1255, 1104, 1019, 798 cm⁻¹. ¹H NMR (300 MHz, DMSO-d₆, δ): 8.25 (s broad, 2H, NH: exchanges with D₂O); 7.32-7.25 (m, 4H, aromatic protons); 7.18-7.14 (m, 4H, aromatic protons); 6.98-6.88 (m, 8H, aromatic protons); 3.78 (s, 12H, OCH₃); 3.62 (s, 4H, CH₂CO); 3.28 (s, 4H, NHCH₂). ¹³C NMR (75 MHz, DMSO-d₆, δ): 167.06, 164.49, 160.66, 159.39, 131.36, 129.82, 121.82, 121.37, 117.01, 114.69, 114.61, 55.65, 55.54, 40.87, 38.94, 33.26. HRMS (ESI) *m/z* calcd for [C₄₀H₃₈N₄O₈ + Na]⁺: 725.4738; found 725.4735.

***N,N'*-(Butane-1,4-diyl)bis{2-[3,4-bis(4-methoxyphenyl)isoxazol-5-yl]acetamide}** (**10**). 83 % Yield. Mp 163-166 °C (EtOAc/Hexane, white solid). FT-IR (KBr): 3836, 3736, 3294, 2930, 1647, 1384, 1287, 1256, 1178, 1097, 1031, 1019, 826, 802 cm⁻¹. ¹H NMR (300 MHz, CDCl₃, δ): 7.42-7.36 (m, 4H, aromatic protons); 7.19-7.13 (m, 4H, aromatic protons); 6.93-6.88 (m, 4H, aromatic protons); 6.85-6.82 (m, 4H, aromatic protons); 6.10 (m, 2H, NH: exchange with D₂O); 3.82 (s, 6H, OCH₃); 3.80 (s, 6H, OCH₃); 3.67 (s, 4H, CH₂CO); 3.29-3.27 (m, 4H, NHCH₂); 1.53-1.49 (m, 4H, CH₂CH₂). ¹³C NMR (75 MHz, CDCl₃, δ): 167.0, 162.9, 161.3, 160.8, 159.6, 131.3, 130.0,

121.6, 121.2, 117.7, 114.5, 115.2, 55.5, 55.4, 39.6, 34.3, 26.8. HRMS (ESI) m/z calcd for $[C_{42}H_{42}N_4O_8 - H]^-$: 729.7875; found 729.7874.

***N,N'*-(Hexane-1,6-diyl)bis{2-[3,4-bis(4-methoxyphenyl)isoxazol-5-yl]acetamide}** (11). The product was isolated by column chromatography (silica gel; mobile phase: $CHCl_3/MeOH = 11:1$). Mp 159-161 °C (yellow solid). 25% Yield. FT-IR (KBr): 3834, 3733, 2924, 1644, 1509, 1384, 1259, 1174, 1100, 1031, 800 cm^{-1} . 1H NMR (500 MHz, $CDCl_3$, δ): 7.40-7.37 (m, 4H, aromatic protons); 7.18-7.16 (m, 4H, aromatic protons); 6.92-6.90 (m, 4H, aromatic protons); 6.86-6.84 (m, 4H, aromatic protons); 6.08-6.04 (m, 2H, *NH*: exchange with D_2O); 3.83 (s, 6H, OCH_3); 3.81 (s, 6H, OCH_3); 3.67 (s, 4H, CH_2CO); 3.29-3.25 (m, 4H, $NHCH_2$); 1.54-1.48 (m, 4H, $NHCH_2CH_2$); 1.36-1.29 (m, 4H, $NH(CH_2)_2CH_2$). ^{13}C NMR (75 MHz, $CDCl_3$, δ): 174.0, 170.1, 168.6, 156.5, 139.8, 136.6, 133.8, 131.4, 131.1, 130.5, 129.5, 115.4, 113.0, 112.6, 100.9, 56.0, 51.8, 39.3, 33.5, 32.5, 29.1, 19.8. HRMS (ESI) m/z calcd for $[C_{44}H_{46}N_4O_8 + Na]^+$: 781.5793; found 781.5798.

***N,N'*-(Dodecane-1,12-diyl)bis{2-[3,4-bis(4-methoxyphenyl)isoxazol-5-yl]acetamide}** (12). The product was isolated by column chromatography (silica gel; mobile phase: $CHCl_3/MeOH = 15:1$). Mp 134-138 °C (yellow solid). 67% Yield. FT-IR (KBr): 3715, 3600, 2929, 2863, 1646, 1609, 1553, 1513, 1428, 1251, 1177, 1037, 831 cm^{-1} . 1H NMR (500 MHz, $CDCl_3$, δ): 7.41-7.39 (m, 4H, aromatic protons); 7.17-7.15 (m, 4H aromatic protons); 6.93-6.91 (m, 4H, aromatic protons); 6.87-6.84 (m, 4H, aromatic protons); 5.75-5.65 (m, 2H, *NH*: exchange with D_2O); 3.84 (s, 4H, CH_2CO); 3.29-3.24 (m, 4H, $NHCH_2CH_2$); 1.57-1.30 (m, 4H, $NH-CH_2CH_2$); 1.28-1.24 (m, 16H). ^{13}C NMR (300 MHz, $CDCl_3$, δ): 162.7, 161.1, 160.6, 159.4, 131.0, 129.7, 121.3, 120.0, 117.4, 114.3, 113.9, 55.2, 40.0, 34.2, 29.3, 29.1, 26.7. HRMS (ESI) m/z calcd for $[C_{50}H_{58}N_4O_8 + Na]^+$: 865.7376; found 865.7377.

***N,N'*-(1,4-Phenylene)bis{2-[3,4-bis(4-methoxyphenyl)isoxazol-5-yl]acetamide}** (13). The product was isolated by column chromatography (silica gel; mobile phase: CHCl₃/MeOH = 15:1). Mp 178-182 °C (pink solid). 45% Yield. FT-IR (KBr): 3749, 3653, 2915, 1639, 1384, 1251, 1107, 821 cm⁻¹. ¹H NMR (500 MHz, DMSO-d₆, δ): 10.30 (bs, 2H, NH: exchange with D₂O); 7.50-7.49 (m, 4H, aromatic protons); 7.30 (d, 4H, *J* = 8.81 Hz, aromatic protons); 7.19 (d, 4H, *J* = 8.32 Hz, aromatic protons); 6.97-6.93 (m, 8H, aromatic protons); 3.84 (s, 4H, CH₂); 3.75 (s, 12H, OCH₃). ¹³C NMR (75 MHz, DMSO-d₆, δ): 165.47, 164.34, 160.74, 160.67, 159.42, 134.94, 131.37, 129.84, 121.72, 121.26, 120.15, 117.21, 114.73, 114.64, 55.64, 55.55, 34.16, 29.45. HRMS (ESI) *m/z* calcd for [C₄₄H₃₈N₄O₈ - H]⁻: 749.7875; found: 749.7872.

***N,N'*-[1,4-Phenylenebis(methylene)]bis{2-[3,4-bis(4-methoxyphenyl)isoxazol-5-yl]acetamide}** (14). The product was isolated by column chromatography (silica gel; mobile phase: CHCl₃/MeOH = 15:1). Mp 168-172 °C (white solid). 26% Yield. ¹H NMR (300 MHz, DMSO-d₆, δ): 8.75-8.65 (m, 2H, NH: exchange with D₂O); 7.34-7.28 (m, 4H, aromatic protons); 7.25-7.12 (m, 8H, aromatic protons); 6.98-6.90 (m, 8H, aromatic protons); 4.28-4.22 (m, 4H, CH₂NH); 3.75 (s, 6H, OCH₃); 3.74 (s, 6H, OCH₃); 3.66 (s, 4H, CH₂CO). ¹³C NMR (75 MHz, DMSO-d₆, δ): 166.84, 164.64, 160.67, 159.41, 138.14, 131.38, 129.82, 127.8, 114.69, 114.64, 79.64, 55.66, 55.56, 42.69, 33.23. HRMS (ESI) *m/z* calcd for [C₄₆H₄₂N₄O₈ + Na]⁺: 801.5693; found: 801.5695.

***N,N'*-(1,1'-biphenyl)-4,4'-diyl]bis{2-[3,4-bis(4-methoxyphenyl)isoxazol-5-yl]acetamide}**(15).

The product was isolated by column chromatography (silica gel; mobile phase: CHCl₃/MeOH = 9:1). Mp 240-243 °C (yellow solid). 26% Yield. FT-IR (KBr): 3715, 3658, 2922, 1605, 1244, 1170, 1026, 827 cm⁻¹. ¹H NMR (500 MHz, DMSO-d₆, δ) : 10.41 (bs, 2H, NH: exchange with D₂O); 7.64-7.60 (m, 8H, aromatic protons); 7.31 (d, 4H, *J* = 8.81 Hz, aromatic protons); 7.19 (d, 4H, *J* = 8.31, aromatic protons); 6.98-6.94 (m, 8H, aromatic protons); 3.88 (s, 4H, CH₂CO); 3.75 (s, 12H, OCH₃). ¹³C NMR (75 MHz, DMSO-d₆, δ): 165.76, 164.29, 160.75, 160.68, 159.44,

138.34, 135.20, 131.37, 129.84, 127.01, 121.72, 121.26, 120.05, 117.28, 114.76, 114.65, 79.62, 55.65, 55.55, 34.28. HRMS (ESI) m/z calcd for $[C_{50}H_{42}N_4O_8 - H]^-$: 825.8831; found 825.8834.

Synthesis of (5Z, 8Z, 11Z, 14Z)-N-(4-{2-[3,4-bis(4-methoxyphenyl)isoxazol-5-yl]acetamido}butyl)icosa-5,8,11,14-tetraenamide (19).

***tert*-Butyl (4-aminobutyl)carbamate (3a).** Butane-1,4-diamine (**3**) (5 g, 56.72 mmol) was solubilized in anhydrous dioxane (40 mL) in an argon-flushed three-necked round bottom flask, equipped with a magnetic stirrer. Then, a solution of di-*tert*-butyl-carbonate (2.48 g, 11.34 mmol) in anhydrous dioxane (40 mL) was very slowly added by a dropping funnel. The obtained turbid reaction mixture was stirred overnight (16 h) at room temperature. Then, the solvent was distilled under reduced pressure and water (50 mL) was added to precipitate the solid di-*tert*-butyl dicarbamate by-product, in turn filtered off. The aqueous solution was extracted with CH_2Cl_2 (5 x 30 mL), and the combined organic phases were dried with anhydrous Na_2SO_4 , filtered and the solvent removed under reduced pressure. *tert*-Butyl (4-aminobutyl)carbamate (**3a**) was isolated as a yellow solid (yield = 79%). FT-IR (KBr): 3359, 2976, 2933, 2866, 1694, 1528, 1453, 1391, 1365, 1276, 1252, 1174, 1042, 989, 867, 781 cm^{-1} . 1H NMR (400 MHz, $CDCl_3$, δ): 5.14 (s, 1H, NH: exchanges with D_2O); 2.94 (q, 2H, $J = 6.4$ Hz); 2.53 (t, 2H, $J = 6.4$ Hz); 1.36-1.26 (m, 6H); 1.07 (s, 9H).

***tert*-Butyl {4-[2-(3,4-bis[4-methoxyphenyl]isoxazol-5-yl)acetamido]butyl}carbamate (3b).** In a three necked-flask (50 mL) equipped with a magnetic stirrer, mofezolac (0.5 g, 1.47 mmol) was solubilized in dry DMF (35 mL). Then, *tert*-butyl (4-aminobutyl)carbamate (**3a**) (0.8 g, 4.25 mmol), 1-hydroxybenzotriazole monohydrate ($HOBt \cdot H_2O$, 309 mg, 1.80 mmol), *N,N*-diisopropylethylamine (0.74 mL, 4.25 mmol), 1-(3-dimethylaminopropyl)-3-ethylcarbodiimide hydrochloride ($EDC \cdot HCl$, 294 mg, 1.54 mmol) were added, and the reaction mixture was stirred overnight (16h) at room temperature. Then, water (30 mL) was added, and the aqueous solution

was extracted with EtOAc (5 x 30 mL). The combined organic extracts were washed with brine, and dried with anhydrous Na₂SO₄, filtered and the solvent distilled under reduced pressure. The product (**3b**) was isolated (65 % yield) by column chromatography (silica gel; mobile phase: EtOAc/MeOH = 95:5). ¹H NMR (400 MHz, CDCl₃, δ): 7.41-7.36 (m, 2H, aromatic protons); 7.18-7.14 (m, 2H, aromatic protons); 6.93-6.89 (m, 2H, aromatic protons); 6.87-6.82 (m, 2H, aromatic protons); 6.01 (s, 1H, CONH: exchanges with D₂O); 4.56 (s, 1H, NH: exchanges with D₂O); 3.83 (s, 3H, OCH₃); 3.80 (s, 3H, OCH₃); 3.68 (s, 2H, CH₂CO); 3.29-3.27 (q, 2H, *J* = 6.4 Hz, CONHCH₂); 3.11-3.13 (q, 2H, *J* = 6.4 Hz, CH₂NHCO); 1.50-1.53 (m, 4H, CH₂CH₂); 1.43 (s, 9H). HRMS (ESI) *m/z* calcd for [C₂₈H₃₅N₃O₆ + Na]⁺: 532.3171; found 532.3172.

4-{2-[3,4-Bis(4-methoxyphenyl)isoxazol-5-yl]acetamido}butan-1-aminium chloride (3c). In a three necked-flask (100 mL) equipped with a magnetic stirrer, *tert*-butyl{4-[2-(3,4-bis[4-methoxyphenyl]isoxazol-5-yl)acetamido]butyl}carbamate (**3b**) (120 mg, 0.236 mmol) was solubilized in CH₂Cl₂ (9 mL), then HCl (g) was bubbled into the yellow reaction mixture for 1h at 25 °C. The reaction progress was monitored by TLC (silica gel, mobile phase: CHCl₃/MeOH = 95:5) until the disappearance of substrate. The product (**3c**) was isolated by removing the solvent under reduced pressure (92 % yield) and used for the next reaction without any further purification). ¹H NMR (400 MHz, CDCl₃, δ): 7.99 (s, 3H, NH₃⁺: exchange with D₂O); 7.35-7.40 (m, 2H, aromatic protons); 7.14-7.18 (m, 2H, aromatic protons); 6.81-6.92 (m, 4H, aromatic protons); 3.80 (s, 3H, OCH₃); 3.82 (s, 3H, OCH₃); 3.67 (s, 2H, CH₂CO); 3.24-3.30 (q, 2H, CH₂); 2.69-2.73 (t, 2H, CONHCH₂); 1.45-1.61 (m, 4H, CCH₂CH₂C).

***N*-(4-Aminobutyl)-2-[3,4-bis(4-methoxyphenyl)isoxazol-5-yl]acetamide (16).** In a round bottom flask 2N Na₂CO₃ was added to a solution of 4-{2-[3,4-bis(4-methoxyphenyl)isoxazol-5-yl]acetamido}butan-1-aminium chloride (**3c**) in EtOAc (3 mL) and the suspension was stirred for 15 minutes at room temperature. Then, the organic phase was treated with anhydrous Na₂SO₄,

filtered and the solvent distilled under reduced pressure. The product was isolated as a yellow oil. ^1H NMR (400 MHz, CDCl_3 , δ): 7.35-7.40 (m, 2H, aromatic protons); 7.30-7.20 (bs, 2H, NH: exchange with D_2O); 7.14-7.18 (m, 2H, aromatic protons); 6.81-6.92 (m, 4H, aromatic protons); 3.82 (s, 3H, OCH_3); 3.80 (s, 3H, OCH_3); 3.67 (s, 2H, CH_2CO); 3.23-3.28 (q, 2H, CH_2); 2.70-2.74 (t, 2H, CONHCH_2); 1.47-1.63 (m, 4H, $\text{CCH}_2\text{CH}_2\text{C}$).

(5Z, 8Z, 11Z, 14Z)-N-(4-{2-[3,4-bis(4-methoxyphenyl)isoxazol-5-yl]acetamido}butyl)icosa-5,8,11,14-tetraenamide (19). Arachidonic acid (0.027 mL, $d = 0.922$ g/mL, 0.082 mmol) was solubilized in anhydrous CH_2Cl_2 (8 mL) in an argon-flushed three-necked round bottom flask, with a dropping funnel and an argon inlet, equipped with a magnetic stirrer and an ice-bath. 1-Hydroxybenzotriazole monohydrate ($\text{HOBt}\cdot\text{H}_2\text{O}$, 28 mg, 0.164 mmol) and 1-(3-dimethylaminopropyl)-3-ethylcarbodiimide hydrochloride ($\text{EDC}\cdot\text{HCl}$, 31.4 mg, 0.164 mmol) were added, and the reaction mixture was stirred at 0°C for 2h. Then, *N*-(4-aminobutyl)-2-[3,4-bis(4-methoxyphenyl)isoxazol-5-yl]acetamide (67 mg, 0.164 mmol) and *N,N*-diisopropylethylamine (0.029 mL, 0.164 mmol) were added, and the reaction mixture was stirred overnight at room temperature. After the disappearance of the starting material, monitored by TLC (silica gel; mobile phase: $\text{CHCl}_3/\text{MeOH} = 9:1$), sat. aq. NaHCO_3 (90 mL) was added to the reaction mixture. Then, after the addition of sat. aq. NH_4Cl (3 x 30 mL), the organic phase was dried with anhydrous Na_2SO_4 , filtered and the solvent removed under reduced pressure at room temperature. The product was isolated by column chromatography (silica gel; mobile phase: $\text{CHCl}_3/\text{MeOH} = 9:1$) in 73% yield. Mp $97-99^\circ\text{C}$. FT-IR (KBr): 3439, 2929, 1649, 1251 cm^{-1} . ^1H NMR (400 MHz, CDCl_3 , δ): 7.40-7.37 (m, 2H, aromatic protons); 7.19-7.16 (m, 2H, aromatic protons); 6.93-6.83 (m, 4H, aromatic protons); 6.20-6.16 (m, 1H, CONH: exchange with D_2O); 5.65-5.62 (m, 1H, NHCO: exchange with D_2O); 5.42-5.31 (m, 8H, $\text{CH}=\text{CH}$); 3.83 (s, 3H, OCH_3); 3.80 (s, 3H, OCH_3); 3.69 (s, 2H, CH_2CONH); 3.33-3.23 (m, 4H, $\text{CONHCH}_2\text{CH}_2\text{CH}_2\text{CH}_2\text{NHCO}$); 2.85-2.79 (m, 6H); 2.19-

2.01 (m, 6H); 1.75-1.65 (m, 2H); 1.63-1.50 (m, 4H); 1.37-1.25 (m, 4H); 0.90-0.85 (t, 3H, CH_3).

HRMS (ESI) m/z calcd for $[C_{43}H_{57}N_3O_5 + Na]^+$: 718.6511; found: 718.6510.

Synthesis of (5Z, 8Z, 11Z, 14Z)-N-(4-{2-[3,4-bis(4-methoxyphenyl)isoxazol-5-yl]acetamido}phenyl)icosa-5,8,11,14-tetraenamide (20).

N-(4-Aminophenyl)-2-[3,4-bis(4-methoxyphenyl)isoxazol-5-yl]acetamide (17). Mofezolac (50 mg, 0.147 mmol) was stirred in anhydrous CH_2Cl_2 (4 mL) in an argon-flushed three-necked round bottom flask kept in an ice-bath at 0 °C equipped with a dropping funnel and an argon inlet. Then, 1-hydroxybenzotriazole monohydrate ($HOBt \cdot H_2O$, 20 mg, 0.147 mmol) and 1-(3-dimethylaminopropyl)-3-ethylcarbodiimide hydrochloride ($EDC \cdot HCl$, 28 mg, 0.147 mmol) were added. The obtained reaction mixture was stirred at 0° C for 2 h. In a dropping funnel was charged a solution of *p*-phenylenediamine (16 mg, 0.147) and *N,N*-diisopropylethylamine (0.025 ml, 0.147 mmol) in anhydrous CH_2Cl_2 (2 mL), previously stirred at room temperature for 30 minutes in a round bottom flask under argon atmosphere. This solution was very slowly dropwise added to the reaction mixture, in turn, then, stirred at room temperature overnight (16h). The solvent was removed under reduced pressure and *N*-(4-aminophenyl)-2-[3,4-bis(4-methoxyphenyl)isoxazol-5-yl]acetamide was isolated by column chromatography (silica gel; mobile phase: $CHCl_3/MeOH=9:1$) as a yellow solid (50 % yield). Mp 202-204 °C. 1H NMR (400 MHz, $CDCl_3$, δ): 7.42-7.40 (m, 2H, aromatic protons); 7.35-7.25 (bs, 1H, *NH*: exchanges with D_2O); 7.25-7.19 (m, 4H, aromatic protons); 6.94-6.92 (m, 2H, aromatic protons); 6.87-6.85 (m, 2H, aromatic protons); 6.66-6.64 (m, 2H, aromatic protons); 3.84 (s, 3H, OCH_3); 3.83 (s, 2H, CH_2CO); 3.82 (s, 3H, OCH_3); 3.62 (s, 2H, NH_2 : exchange with D_2O). HRMS (ESI) m/z calcd for $[C_{25}H_{23}N_3O_4 + Na]^+$: 452.1930; found: 452.1930.

(5Z, 8Z, 11Z, 14Z)-N-(4-{2-[3,4-Bis(4-methoxyphenyl)isoxazol-5-yl]acetamido}phenyl)icosa-5,8,11,14-tetraenamide (20). Arachidonic acid (0.012 mL, $d =$

0.922 g/mL, 0.038 mmol) was solubilized in anhydrous CH_2Cl_2 (2 mL) in an argon-flushed three-necked round bottom flask, kept in an ice-bath at 0°C equipped with a dropping funnel and an argon inlet. 1-Hydroxybenzotriazole monohydrate ($\text{HOBt}\cdot\text{H}_2\text{O}$, 20 mg, 0.147 mmol) and 1-(3-dimethylaminopropyl)-3-ethylcarbodiimide hydrochloride ($\text{EDC}\cdot\text{HCl}$, 28 mg, 0.147 mmol) were added, and the reaction mixture was stirred at 0°C for 2 h. In a dropping funnel was charged a solution of *N*-(4-aminophenyl)-2-[3,4-bis(4-methoxyphenyl)isoxazol-5-yl]acetamide (16 mg, 0.147) and *N,N*-diisopropylethylamine (0,025 mL, 0,147 mmol) in anhydrous CH_2Cl_2 (2 mL) previously stirred at room temperature for 30 minutes in a round bottom flask under argon atmosphere. This solution was very slowly dropwise added to the reaction mixture, in turn stirred at room temperature overnight (16h). Then, a sat. aq. NaHCO_3 (8 mL) was added, and after separation from the aqueous solution, the organic phase was dried over anhydrous Na_2SO_4 , filtered and the solvent removed under reduced pressure at room temperature. The product was isolated by column chromatography (silica gel; mobile phase: $\text{CHCl}_3/\text{MeOH} = 9:1$). 85 % Yield. Mp $133\text{-}135^\circ\text{C}$. ^1H NMR (400 MHz, CDCl_3 , δ): 7.50-7.40 (m, 7H, 6 aromatic protons and *NHCO*); 7.22-7.19 (m, 2H, aromatic protons); 7.09 (s, 1H, *NHCO*: exchanges with D_2O); 6.96-6.92 (m, 2H, aromatic protons); 6.88-6.84 (m, 2H, aromatic protons); 5.44-5.32 (m, 8H, *CH=CH*); 3.85 (s, 2H, CH_2CONH); 3.84 (s, 3H, OCH_3); 3.81 (s, 3H, OCH_3); 2.86-2.78 (m, 6H); 2.38-2.34 (m, 2H); 2.20-2.15 (m, 2H); 2.09-2.02 (m, 2H); 1.86-1.80 (m, 2H); 1.37-1.24 (m, 6H); 0.92-0.80 (m, 3H, CH_3); ^{13}C NMR (75 MHz, CDCl_3 , δ): 164.48, 162.06, 161.25, 160.71, 159.61, 134.67, 133.47, 131.08, 130.52, 129.79, 128.98, 128.60, 128.27, 128.10, 127.82, 127.51, 121.19, 120.89, 120.41, 117.80, 114.50, 114.01, 55.25, 36.94, 35.13, 31.91, 31.49, 30.90, 29.68, 29.30, 27.20, 26.59, 25.64, 25.25, 22.55, 14.06. HRMS (ESI) m/z calcd for $[\text{C}_{45}\text{H}_{53}\text{N}_3\text{O}_5 + \text{Na}]^+$: 738.6412; found: 738.6415.

Synthesis of (5Z, 8Z, 11Z, 14Z)-N-(4'-[2-[3,4-bis(4-methoxyphenyl)isoxazol-5-yl]acetamido]-[1,1'-biphenyl]-4-yl)icosa-5,8,11,14-tetraenamide (21).

N-[4'-Amino-(1,1'-biphenyl)-4-yl]-2-[3,4-bis(4-mehoxyphenyl)isoxazol-5-yl]acetamide (18).

Mofezolac (50 mg, 0.143 mmol) was solubilized in anhydrous CH₂Cl₂ (4 mL) in an argon-flushed three-necked round bottom flask, equipped with a dropping funnel and an argon inlet, and kept in an ice-bath at 0 °C. 1-Hydroxybenzotriazole monohydrate (HOBt·H₂O, 20 mg, 0,147 mmol) and 1-(3-dimethylaminopropyl)-3-ethylcarbodiimide hydrochloride (EDC·HCl, 28 mg, 0.147 mmol) were added, and the reaction mixture was stirred at 0 °C for 2 h. In a dropping funnel was charged a solution of benzidine (27 mg, 0.147 mmol) and *N,N*-diisopropylethylamine (0,025 mL, 0,147 mmol) in anhydrous CH₂Cl₂ (2 mL), previously stirred at room temperature for 30 minutes in a round bottom flask under argon atmosphere. This solution was very slowly dropwise added to the reaction mixture, in turn stirred at room temperature overnight (16h). A sat. aq. NaHCO₃ (9 mL) was then added, and after separation from the aqueous solution, the organic phase was dried over anhydrous Na₂SO₄, filtered and the solvent removed under reduced pressure at room temperature. The *N*-(4'-amino-[1,1'-biphenyl]-4-yl)-2-[3,4-bis(4-mehoxyphenyl)isoxazol-5-yl]acetamide was isolated by column chromatography (silica gel; mobile phase: CHCl₃/MeOH = 10:1). 27 % Yield. Mp 204-206 °C. ¹H NMR (500 MHz, CDCl₃, δ): 7.52-7.49 (m, 5H, 4H aromatic protons, and 1H, NH: exchanges with D₂O); 7.42-7.33 (m, 4 H, aromatic protons); 7.21 (d, 2H, *J* = 8.81 Hz, aromatic protons); 6.95 (d, 2H, *J* = 8.81, aromatic protons); 6.87 (d, 2H, *J* = 8.81, aromatic protons); 6.75 (d, 2H, *J* = 8.32, aromatic protons); 3.88 (s, 2H, CH₂CO); 3.85 (s, 3H, OCH₃); 3.82 (s, 3H, OCH₃); 3.66-3.63 (bs, 2H, NH₂: exchange with D₂O). ¹³C NMR (125 MHz, CDCl₃, δ): 159.67; 157.32; 156.55; 155.96; 154.87; 141.06; 133.08; 130.81; 126.35; 125.99; 125.07; 123.0; 122.05; 116.43; 116.12; 115.69; 113.07; 110.64; 109.77; 109.28; 58.38; 50.55; 30.51. HRMS (ESI) *m/z* calcd for [C₃₁H₂₇N₃O₄ + Na]⁺: 528.2885; found: 528.2884.

(5Z, 8Z, 11Z, 14Z)-*N*-{4'-{2-[3,4-Bis(4-methoxyphenyl)isoxazol-5-yl]acetamido}-(1,1'-biphenyl)-4-yl}icosa-5, 8, 11, 14-tetraenamide (**21**). Arachidonic acid (0.011 mL, 0.033 mmol) was solubilized in anhydrous CH₂Cl₂ (2 mL) in an argon-flushed three-necked round bottom flask, equipped with a dropping funnel and an argon inlet, and kept in an ice-bath. 1-Hydroxybenzotriazole monohydrate (HOBt·H₂O, 6 mg, 0.039 mmol) and 1-(3-dimethylaminopropyl)-3-ethylcarbodiimide hydrochloride (EDC·HCl, 8 mg, 0.039 mmol) were added, and the reaction mixture was stirred at 0 °C for 2 h. In a dropping funnel was charged a solution of *N*-[4'-amino-(1,1'-biphenyl)-4-yl]-2-[3,4-bis(4-methoxyphenyl)isoxazol-5-yl]acetamide (20 mg, 0.039) and *N,N*-diisopropylethylamine (0.007 mL, 0.039 mmol) were solubilized in anhydrous CH₂Cl₂ (2 mL) previously stirred at room temperature for 30 minutes in a round bottom flask under argon atmosphere. This solution was very slowly dropwise added to the reaction mixture, in turn stirred at room temperature overnight (16h). Then, a sat. aq. NaHCO₃ (10 mL) was added to the reaction mixture and, after separation from the aqueous solution, the obtained organic phase was dried over anhydrous Na₂SO₄, filtered and the solvent removed under reduced pressure at room temperature. The product was isolated by column chromatography (silica gel; mobile phase: CHCl₃/MeOH = 10:1). 31 % Yield. Mp 132-134 °C. ¹H NMR (600 MHz, DMSO-d₆, δ): 10.42-10.38 (bs, 1H, CONH: exchanges with D₂O); 9.95-9.89 (bs, 1H, CONH: exchanges with D₂O); 7.68-7.55 (m, 8H, aromatic protons); 7.32 (d, 2H, *J* = 8.41 Hz, aromatic protons); 7.21 (d, 2H, *J* = 8.40 Hz, aromatic protons); 7.01-6.94 (m, 4H, aromatic protons); 5.45-5.28 (m, 8H, CH=CH); 3.89 (s, 2H, CH₂CONH); 3.75 (s, 6H, OCH₃); 2.86-2.75 (m, 6H); 2.35-2.31 (m, 2H); 2.14-2.08 (m, 2H); 2.05-1.98 (m, 2H); 1.72-1.64 (m, 2H); 1.32-1.18 (m, 6H); 0.83 (t, 3H, *J* = 6.6 Hz, CH₃). ¹³C NMR (125 MHz, CDCl₃, δ): 171.07, 164.58, 162.06, 161.31, 160.71, 159.62, 137.00, 136.39, 131.11, 130.54, 129.96, 129.81, 129.00, 128.62, 128.30, 129.12, 127.84, 127.54, 127.51, 127.32, 127.28, 121.18, 120.85, 120.49, 120.13, 117.86, 114.51,

114.03, 63.12, 63.10, 55.30, 55.26, 37.04, 35.26, 32.82, 31.93, 31.91, 31.51, 29.77, 29.70, 29.50, 27.2, 26.60, 25.74, 25.29, 22.68, 14.12. HRMS (ESI) m/z calcd for $[C_{51}H_{57}N_3O_5 + Na]^+$: 814.7367; found: 814.7370.

Cyclooxygenase activity inhibition determination. Preliminarily, the new compounds were evaluated for their ability to inhibit ovine COX-1 or human COX-2 enzyme measuring the extent (%) of enzyme activity inhibition at 50 μ M. The inhibition of the enzyme was evaluated by using a colorimetric COX inhibitor screening assay kit (Catalog No. 7601050, Cayman Chemicals, Ann Arbor, MI, USA) following the manufacturer's instructions. COX is a bifunctional enzyme exhibiting both cyclooxygenase and peroxidase activities. The cyclooxygenase component catalyzes the conversion of arachidonic acid into the hydroperoxide PGG₂, and then peroxidase component catalyzes PGG₂ reduction into the corresponding alcohol PGH₂, the precursor of PGs, thromboxane and prostacyclin. The Colorimetric COX Inhibitor Screening Assay colorimetrically measures the peroxidase activity of the cyclooxygenases monitoring the appearance of oxidized *N,N,N',N'*-tetramethyl-*p*-phenylenediamine (TMPD) at $\lambda = 590$ nm. Stock solutions of test compounds were dissolved in DMSO.

Antiplatelet Assays. Human platelet rich (PRP) and poor (PPP) plasma were prepared by differential centrifugation of the whole blood (n=3) and the platelet aggregation was monitored by turbidimetric method using Chrono-log 560VS Aggregometer (Chrono-Log, Havertown, PA, USA). The derivatives were pre-incubated in PRP for two min before addition of the arachidonic acid (AA - 500 μ M) (Cayman Chemical Company, Ann Arbor, MI, USA). Different concentrations of the compounds were also tested to determine the concentration required to inhibit 50% of platelet aggregation (IC₅₀) induced by AA. The platelet aggregation tests were performed in triplicate and the positive controls were acetylsalicylic acid (ASA) (Sigma Aldrich,

SP, Brazil) and the negative control was the vehicle dimethyl sulfoxide (DMSO 1%) (Sigma Aldrich, SP, Brazil)³⁹.

Anticoagulant Assays. Human platelet poor (PPP) plasma was prepared by differential centrifugation of the whole blood (n=3) and the assays were performed in coagulation analyzer CoagLab® IV (Beijing Shining Sun Technology Co. Ltd., China) as described by Sathler *et al.*⁴⁰. In the aPTT assay, plasma samples were first incubated with the compounds (100 µM) for 15 minutes at room temperature and then for 2 minutes at 37 °C. Next, cephalin (100 µl) was added and incubated for 2 minutes. The reaction was triggered with 100 µl of 0.025 M CaCl₂ in a final volume of 300µL. In the PT test, similarly, 97 µL of plasma were first incubated with the compounds for 15 minutes at room temperature and then 2 minutes at 37 °C. Then 100 µL of PBS were added and incubated for 3 minutes. The reaction was triggered with 100 µL of calcium thromboplastin, in a final volume of 300 µL. The plasma clotting time was monitored in seconds at 37 °C.

Hemolytic Activity. The hemolytic activity of compounds was investigated according to Parnham and Wetzig^{41,42}. The citrated blood (n=3) was centrifuged at 2500 rpm for 15 minutes and the erythrocyte pellet was washed 3 times with PBS (pH 7.4) and resuspended in the same buffer. Then the derivatives were incubated with the suspension of erythrocytes for 3h at 37 °C in accord to ASTM F756-00 (Standard Practice for Assessment of Hemolytic Properties of Materials). The release of hemoglobin was measured after centrifugation of samples (2500 rpm for 15 min) and checked in a spectrophotometer at 540 nm. The complete hemolysis was obtained using 1% Triton X-100 as positive control. Less than 10% hemolysis was considered non-hemolytic³⁷.

Cytotoxicity to Vero cell line. Vero cell line, from kidney epithelial cells extracted from an African green monkey (*Chlorocebus* sp), was purchased from the Rio de Janeiro Cell Bank, Brazil. Dulbecco's Modified Eagles Medium (DMEM), Hank's Balanced Salt Solution, fetal bovine serum (FBS), antibiotic solution (10,000U/mL penicillin, 10mg/mL streptomycin), antimycotic solution (25–30µg/mL amphotericin B), trypsin–EDTA solution (2.5mg/mL trypsin, 0.2mg/mL EDTA) and 3-(4,5-dimethylthiazol-2-yl)-2,5-diphenyl tetrazolium bromide (MTT) were all supplied by Sigma–Aldrich (São Paulo, Brazil). Dimethyl sulfoxide (DMSO) and other reagents were from analytical grade. Culture medium was supplemented with 4.5 mg/ml glucose, 0.1 mg/ml penicillin, 0.14 mg/ml streptomycin and 10% inactivated FBS. Cultured cells were maintained at 37°C in an atmosphere containing 95% air and 5% CO₂. Cells were sub-cultivated every 48 h by trypsin–EDTA solution. Metabolically active cells were assessed using the MTT reduction colorimetric assay, as previously reported by Mosmann (1983)⁴³. Cells were seeded in 96-well plates (Corning) at a density of 3.2×10^4 cells/well, distributed in a total volume of 200 µL/well. Then the plates were taken to cell incubator at 37°C and 5% CO₂ for 24 hours. After incubation, the cells were placed in contact with the samples (10 and 100 µM; n = 4) for 48 hours. As control group we used DMEM containing 10% FBS and 1% of DMSO. Then, samples were aspirated and the cells were treated with MTT reagent (2.5 mg/mL) by adding 100 µL of HBSS and 25 µL of MTT solution per well. The plates containing the cells were incubated with MTT for 3 hours at 37°C and 5% CO₂. At the end of incubation time, MTT was aspirated and the cells were washed with phosphate buffer solution (PBS) (pH 7.4). The buffer was aspirated and DMSO was added (100 µL/well) for cell viability measurement by absorbance at 570 nm, after shaking vigorously for 60 seconds, using a microplate reader (TP-Reader™, Thermoplate, Brazil). The cytotoxicity/cell viability was expressed as the percentage of cells surviving in relation to untreated cells⁴⁴.

Genotoxicity Tests. Reverse Mutagenesis to Histidine Prototrophy (Ames Test). This assay was performed as described by Maron and Ames⁴⁵, using the histidine *Salmonella typhimurium* auxotroph mutant strains TA97, TA98, TA100 and the wild type strain TA102. Each assay was conducted in triplicate and the results obtained show a comparison between the molecules and the positive control 4-NQO. The negative results indicated that the molecules have no mutagenic properties.

SOS Chromotest - “Spot Test”. The SOS chromotest (spot test) was performed according to Quillardet and Hofnung⁴⁵, using *Escherichia coli* strains PQ35 and PQ37. One hundred microliters of an overnight culture of the *E. coli* strains are diluted in 5 mL of LB medium and the culture is incubated at 37 °C in a gyratory incubator up to a concentration of 2×10^8 bacteria/mL. Fractions of 0.1 mL of the culture are then distributed into the test tube with top agar, and the mixture is poured immediately on M63 medium plate. A sample of 10 µL of the molecules is spotted onto the center of the plate. After overnight incubation at 37 °C, the presence of a blue ring around a zone of inhibition indicates genotoxic activity. Each assay was conducted in triplicate and the results obtained show a comparison between the molecules and the positive control 4-NQO.

Computational methods. The binding poses in the COX active sites were generated using the FLAP software in the structure-based mode (Molecular Discovery Ltd., UK; www.moldiscovery.com). The procedure has been extensively described in the Supplementary Material. The protein binding site was calculated with the FLAP site module in the FLAP software that is able to reproduce the main cavities of the crystallographic structures. For each ligand a maximum of 25 conformers were generated to mimic the compound flexibility; the protonation

state at physiological pH of each molecule was assigned to ionizable residues, as predicted by MoKa^{46,47}. The FLAP software was used in the “structure-based” mode; this approach allows to generate binding poses of a ligand in a protein cavity based on the similarity between their GRID fields⁴⁸. The GRID Molecular Interaction Fields were generated through the probes for H (shape), DRY (hydrophobic interactions) N1 (H-bond donor) and O (H-bond acceptor) interactions.

Ethics and Compliance

All human blood samples were obtained from adult volunteers, healthy, 21-35 years, without use of drugs or other substances that could interfere with the experiment for at least 15 days (Ethics Committee – ID number: 2.364.834)

Author Contributions

The manuscript was written through the contribution of all authors. All authors approved the final version of the manuscript. The authors declare no competing financial interest.

ACKNOWLEDGMENTS

This work was supported by First AIRC Grant-MFAG2015 (Project Id. 17566). We thank the financial support of Fundação de Amparo à Pesquisa do Estado do Rio de Janeiro (FAPERJ), Conselho Nacional de Desenvolvimento Científico e Tecnológico (CNPq) and Coordenação de Aperfeiçoamento de Pessoal Docente (CAPES).

ABBREVIATIONS USED

AA, arachidonic acid; COX, cyclooxygenases; NSAIDs, Non-Steroidal Anti-inflammatory Drugs; PG, prostaglandin; TX, thromboxane; FLAP: Fingerprints for Ligands and Proteins.

REFERENCES

- [1] P. Macek, M. Zak, M. Terek-Derszniak, M. Biskup, P. Ciepiela, H. Krol, J. Smok-Kalwat, S. Gozdz, Age-dependent disparities in the prevalence of single and clustering cardiovascular risk factors: A cross-sectional cohort study in middle-aged and older adults, *Clin. Interv. Aging.* 15 (2020) 161–169. doi: 10.2147/CIA.S238930.
- [2] F. Jiang, Y. Zhu, C. Gong, X. Wei, Atherosclerosis and Nanomedicine Potential: Current Advance and Future Opportunities, *Curr. Med. Chem.* 27 (2019) 3534–3554. doi:10.2174/0929867326666190301143952.
- [3] E. D'Alessandro, C. Becker, W. Bergmeier, C. Bode, J.H. Bourne, H. Brown, H.R. Buller, A.J. Ten Cate-Hoek, V. Ten Cate, Y.J.M. Van Cauteren, Y.F.H. Cheung, A. Cleuren, D. Coenen, H.J.G.M. Crijns, I. De Simone, S.C. Dolleman, C.E. Klein, D.I. Fernandez, L. Granneman, A. Van T Hof, P. Henke, Y.M.C. Henskens, J. Huang, L.K. Jennings, N. Jooss, M. Karel, D. Van Den Kerkhof, F.A. Klok, B. Kremers, B. Lämmle, A. Leader, A. Lundstrom, N. Mackman, P.M. Mannucci, Z. Maqsood, P.E.J. Van Der Meijden, M. Van Moorsel, L.A. Moran, J. Morser, M. Van Mourik, S. Navarro, R.A.I. Neagoe, R.H. Olie, P. Van Paridon, J. Pasma, I. Provenzale, P.H. Reitsma, B. Scaf, L. Schurgers, J. Seelig, A. Siegbahn, B. Siegerink, O. Soehnlein, E.M. Soriano, M.A. Sowa, H.M.H. Spronk, R.F. Storey, C. Tantiwong, A. Veninga, X. Wang, S.P. Watson, J. Weitz, S.S. Zeerleder, H. Ten Cate, B. Lina, B. Christoph, H. Marc, K. Peter, K. Rory, L. Gregory, M. Steffen, V.H. Philipp, W. Christian, W. Johann, Thrombo-Inflammation in Cardiovascular Disease: An Expert Consensus Document from the Third Maastricht Consensus Conference on Thrombosis, *Thromb. Haemost.* 120 (2020) 538–564. doi: 10.1055/s-0040-1708035. <https://doi.org/10.1055/s-0040-1708035>.
- [4] K. Thygesen, J.S. Alpert, A.S. Jaffe, B.R. Chaitman, J.J. Bax, D.A. Morrow, H.D. White, Fourth Universal Definition of Myocardial Infarction, *Glob. Heart.* 13 (2018) 305–338. doi: 10.1016/j.gheart.2018.08.004.
- [5] M. Centa, H. Jin, L. Hofste, S. Hellberg, A. Busch, R. Baumgartner, N.J. Verzaal, S. Lind Enoksson, L. Perisic Matic, S. V. Boddul, D. Atzler, D.Y. Li, C. Sun, G.K. Hansson, D.F.J. Ketelhuth, U. Hedin, F. Wermeling, E. Lutgens, C.J. Binder, L. Maegdesfessel, S.G. Malin, Germinal Center-Derived Antibodies Promote Atherosclerosis Plaque Size

- and Stability, *Circulation* 139 (2019) 2466–2482. doi: 10.1161/CIRCULATIONAHA.118.038534.
- [6] I. Induruwa, M. Moroi, A. Bonna, J.-D. Malcor, J.-M. Howes, E.A. Warburton, R.W. Farndale, S.M. Jung, Platelet collagen receptor Glycoprotein VI-dimer recognizes fibrinogen and fibrin through their D-domains, contributing to platelet adhesion and activation during thrombus formation, *J. Thromb. Haemost. JTH.* 16 (2018) 389–404. doi: 10.1111/jth.13919. <https://doi.org/10.1111/jth.13919>.
- [7] M. Kannan, F. Ahmad, R. Saxena, Platelet activation markers in evaluation of thrombotic risk factors in various clinical settings, *Blood Rev.* 37 (2019) 100583. doi: 10.1016/j.blre.2019.05.007.
- [8] L. Pujadas-Mestres, I. Lopez-Vilchez, E. Arellano-Rodrigo, J.C. Reverter, A. Lopez-Farre, M. Diaz-Ricart, J.J. Badimon, G. Escolar, Differential inhibitory action of apixaban on platelet and fibrin components of forming thrombi: Studies with circulating blood and in a platelet-based model of thrombin generation, *PLoS One.* 12 (2017) e0171486. doi:10.1371/journal.pone.0171486.
- [9] P. Sabouret, M.P. Savage, D. Fischman, F. Costa, Complexity of Antiplatelet Therapy in Coronary Artery Disease Patients, *Am. J. Cardiovasc. Drugs.* (2020). doi: 10.1007/s40256-020-00414-0. Epub ahead of print.
- [10] M. Tscharrre, A.D. Michelson, T. Gremmel, Novel Antiplatelet Agents in Cardiovascular Disease, *J. Cardiovasc. Pharmacol. Ther.* 25 (2020). 191–200. doi: 10.1177/1074248419899314.
- [11] M Bijak, J. Saluk-Bijak, Flavonolignans Inhibit the Arachidonic Acid Pathway in Blood Platelets, *BMC Complement. Altern. Med.* 17 (2017)396. doi: 10.1186/s12906-017-1897-7.
- [12] C.T. O’connor, T.J. Kiernan, B.P. Yan, The genetic basis of antiplatelet and anticoagulant therapy: A pharmacogenetic review of newer antiplatelets (clopidogrel, prasugrel and ticagrelor) and anticoagulants (dabigatran, rivaroxaban, apixaban and edoxaban), *Expert Opin. Drug Metab. Toxicol.* 13 (2017) 725–739. doi: 10.1080/17425255.2017.1338274.
- [13] A.S. Nathan, S. Sen, R.W. Yeh, The risk of bleeding with the use of antiplatelet agents for the treatment of cardiovascular disease, *Expert Opin. Drug Saf.* 16 (2017) 561–572. doi: 10.1080/14740338.2017.1315101.

- [14] K.R.R. Rengasamy, H. Khan, I. Ahmad, D. Lobine, F. Mahomoodally, S. Suroowan, S.T.S. Hassan, S. Xu, S. Patel, M. Daglia, S.M. Nabavi, S.K. Pandian, Bioactive peptides and proteins as alternative antiplatelet drugs, *Med. Res. Rev.* 39 (2019) 2153-2171. doi: 10.1002/med.21579.
- [15] P. Vitale, S. Tacconelli, M.G. Perrone, P. Malerba, L. Simone, A. Scilimati, A. Lavecchia, M. Dovizio, E. Marcantoni, A. Bruno, P. Patrignani, Synthesis, pharmacological characterization, and docking analysis of a novel family of diarylisoxazoles as highly selective cyclooxygenase-1 (COX-1) inhibitors, *J. Med. Chem.* 56 (2013) 4277-4299. doi:10.1021/jm301905a.
- [16] P. Vitale, M.G. Perrone, P. Malerba, A. Lavecchia, A. Scilimati, Selective COX-1 inhibition as a target of theranostic novel diarylisoxazoles, *Eur. J. Med. Chem.* 74 (2014) 606-618. doi: 10.1016/j.ejmech.2013.12.023.
- [17] M.G. Perrone, P. Vitale, A. Panella, S. Ferorelli, M. Contino, A. Lavecchia, A. Scilimati. Isoxazole-Based-Scaffold Inhibitors Targeting Cyclooxygenases (COXs), *ChemMedChem* 11 (2016) 1172–1187. doi: 10.1002/cmdc.201500439.
- [18] M .G. Perrone, P. Vitale, S. Ferorelli, A. Boccarelli, M. Coluccia, A. Pannunzio, F. Campanella, G. Di Mauro, C. Bonaccorso, C.G. Fortuna, A. Scilimati, Effect of mofezolac-galactose distance in conjugates targeting cyclooxygenase (COX)-1 and CNS GLUT-1 carrier, *Eur. J. Med. Chem.* 141 (2017) 404–416. doi: 10.1016/j.ejmech.2017.09.066.
- [19] G. Cingolani, A. Panella, M.G. Perrone, P. Vitale, G. Di Mauro, C.G. Fortuna, R.S. Armen, S. Ferorelli, W.L. Smith, A. Scilimati, Structural basis for selective inhibition of Cyclooxygenase-1 (COX-1) by diarylisoxazoles mofezolac and 3-(5-chlorofuran-2-yl)-5-methyl-4-phenylisoxazole (P6), *Eur. J. Med. Chem.* 138 (2017) 661-668. doi: 10.1016/j.ejmech.2017.06.045.
- [20] M. G. Perrone, D. D. Lofrumento, P. Vitale, F. De Nuccio, V. La Pesa, A. Panella, R. Calvello, A. Cianciulli, M. A. Panaro, A. Scilimati, Selective Cyclooxygenase-1 Inhibition by P6 and Gastrotoxicity: Preliminary Investigation, *Pharmac.* 95 (2015), 22–28. doi: 10.1159/000369826.
- [21] P. Vitale, A. Panella, A. Scilimati, M.G. Perrone, COX-1 Inhibitors: Beyond Structure Toward Therapy, *Med. Res. Rev.* 36 (2016) 641-671. doi: 10.1002/med.21389.

- [22] M. G. Perrone, A. Scilimati, L. Simone, P. Vitale, Selective COX-1 Inhibition: A Therapeutic Target to be Reconsidered, *Curr. Med. Chem.* 17 (2010) 3769-3805. doi: 10.2174/092986710793205408.
- [23] J.A. Mitchell, N.S. Kirkby, Eicosanoids, prostacyclin and cyclooxygenase in the cardiovascular system, *Br. J. Pharmacol.* 176 (2019) 1038-1050. doi: 10.1111/bph.14167.
- [24] M. Baroni, G. Cruciani, S. Sciabola, F. Perruccio, J.S. Mason, A common reference framework for analyzing/comparing proteins and ligands. Fingerprints for Ligands and Proteins (FLAP): Theory and application, *J. Chem. Inf. Model.* 47 (2007) 279-294. doi:10.1021/ci600253e.
- [25] G. Rimon, R.S. Sidhu, D.A. Lauver, J.Y. Lee, N.P. Sharma, C. Yuan, R.A. Frieler, R.C. Trievel, B.R. Lucchesi, W.L. Smith, COXibs interfere with the action of aspirin by binding tightly to one monomer of cyclooxygenase-1, *Proc. Natl. Acad. Sci. U. S. A.* 107 (2010) 28-33. doi: 10.1073/pnas.0909765106.
- [26] M.G. Malkowski, S.L. Ginell, W.L. Smith, R.M. Garavito, The productive conformation of arachidonic acid bound to prostaglandin synthase, *Science* 289 (2000) 1933-1937. doi:10.1126/science.289.5486.1933.
- [27] J.L. Wang, D. Limburg, M.J. Graneto, J. Springer, J.R.B. Hamper, S. Liao, J.L. Pawlitz, R.G. Kurumbail, T. Maziasz, J.J. Talley, J.R. Kiefer, J. Carter, The novel benzopyran class of selective cyclooxygenase-2 inhibitors. Part 2: The second clinical candidate having a shorter and favorable human half-life, *Bioorganic Med. Chem. Lett.* 20 (2010) 7159-7163. doi: 10.1016/j.bmcl.2010.07.054.
- [28] J.K. Gierse, J.J. McDonald, S.D. Hauser, S.H. Rangwala, C.M. Koboldt, K. Seibert, A single amino acid difference between cyclooxygenase-1 (COX-1) and -2 (COX-2) reverses the selectivity of COX-2 specific inhibitors. *J. Biol. Chem.* 271 (1996) 15810-15814. doi:10.1074/jbc.271.26.15810.
- [29] M.L. Pati, P. Vitale, S. Ferorelli, M. Iaselli, M. Miciaccia, A. Boccarelli, G.D. Di Mauro, C.G. Fortuna, T.F. Souza Domingos, L.C. Rodrigues Pereira da Silva, M. de Pádula, L.M. Cabral, P.C. Sathler, A. Vacca, A. Scilimati, M.G. Perrone, Translational impact of novel widely pharmacological characterized mofezolac-derived COX-1 inhibitors combined with bortezomib on human multiple myeloma cell lines viability, *Eur. J. Med. Chem.* 164 (2019) 59-76. doi: 10.1016/j.ejmech.2018.12.029.

- [30] M.G. Perrone, P. Vitale, S. Ferorelli, A. Boccarelli, M. Coluccia, A. Pannunzio, F. Campanella, G. Di Mauro, C. Bonaccorso, C.G. Fortuna, A. Scilimati, Effect of mofezolac-galactose distance in conjugates targeting cyclooxygenase (COX)-1 and CNS GLUT-1 carrier, *Eur. J. Med. Chem.* 141 (2017) 404–416 doi: 10.1016/j.ejmech.2017.09.066.
- [31] G. Casalino, M. Coluccia, M.L. Pati, A. Pannunzio, A. Vacca, A. Scilimati, M.G. Perrone. Intelligent microarray data analysis through non-negative matrix factorization to study human multiple myeloma cell lines, *Appl. Sci.* 9 (2019) 1-18.
- [32] R. Lordan, A. Tsoupras, I. Zabetakis, Platelet activation and prothrombotic mediators at the nexus of inflammation and atherosclerosis: Potential role of antiplatelet agents, *Blood Rev.* (2020). doi: 10.1016/j.blre.2020.100694.
- [33] M.G. Perrone, P. Malerba, M.J. Uddin, P. Vitale, A. Panella, B.C. Crews, C.K. Daniel, K. Ghebreselasie, M. Nickels, M.N. Tantawy, H.C. Manning, L.J. Marnett, A. Scilimati, PET radiotracer [¹⁸F]-P6 selectively targeting COX-1 as a novel biomarker in ovarian cancer: Preliminary investigation, *Eur. J. Med. Chem.* 80 (2014) 562-568. doi: 10.1016/j.ejmech.2014.04.074.
- [34] A. Scilimati, S. Ferorelli, M.C. Iaselli, M. Miciaccia, M.L. Pati, C.G. Fortuna, A.M. Aleem, L.J. Marnett, M.G. Perrone, Targeting COX-1 by mofezolac-based fluorescent probes for ovarian cancer detection, *Eur. J. Med. Chem.* 179 (2019) 16-25. doi: 10.1016/j.ejmech.2019.06.039.
- [35] M.G. Perrone, O. Luisi, A. De Grassi, S. Ferorelli, G. Cormio, A. Scilimati, Translational Theragnostic of Ovarian Cancer: Where do we stand?, *Curr. Med. Chem.* (2019). doi: 10.2174/0929867326666190816232330. Online ahead of print.
- [36] K. V. Sashidhara, G.R. Palnati, S.R. Avula, S. Singh, M. Jain, M. Dikshit, Synthesis and evaluation of anti-thrombotic activity of benzocoumarin amide derivatives, *Bioorganic Med. Chem. Lett.* 22 (2012) 3115-3121. doi: 10.1016/j.bmcl.2012.03.059.
- [37] D. Fischer, Y. Li, B. Ahlemeyer, J. Krieglstein, T. Kissel, In Vitro Cytotoxicity Testing of Polycations: Influence of Polymer Structure on Cell Viability and Hemolysis. *Bio-materials* 24 (2003) 1121–1131. doi: 10.1016/s0142-9612(02)00445-3.
- [38] M. Rao, M. M. Kumar, M. A Rao, In Vitro and in Vivo Effects of Phenolic Antioxidants against Cisplatin-Induced Nephrotoxicity, *J. Biochem. (Tokyo)* 125 (1999) 383–390. doi: 10.1093/oxfordjournals.jbchem.a022298.

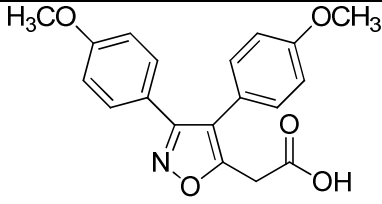
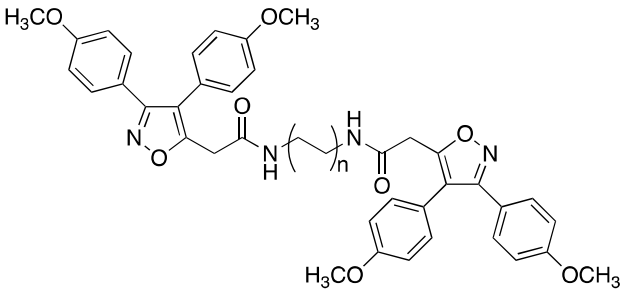
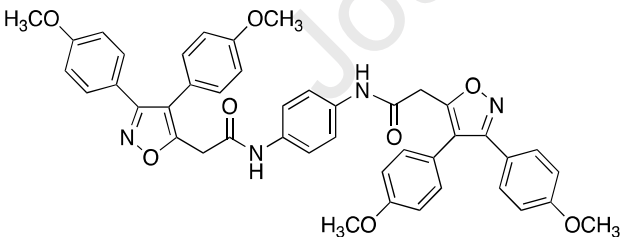
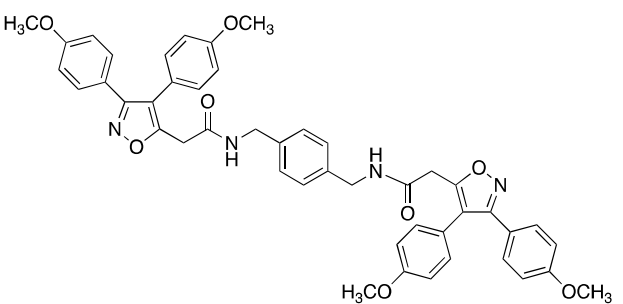
- [39] A. L. Lourenço, R. R. S. Salvador, L. A. Silva, M. S. Saito, J. F. R. Mello, L.M. Cabral, C. R. Rodrigues, M. A. F. Vera, E. M. F. Muri, A. M. T. de Souza, C.S. Craik, L. R. S. Dias, C. H. Castro, P. C Sathler, Synthesis and Mechanistic Evaluation of Novel N'-Benzylidene-Carbohydrazide-1H-Pyrazolo[3,4-b] Pyridine Derivatives as Non-Anionic Antiplatelet Agents, *Eur. J. Med. Chem.* 135 (2017) 213–229. doi: 10.1016/j.ejmech.2017.04.023.
- [40] P.C. Sathler, A.L. Lourenço, C.R. Rodrigues, L.C.R.P. Da Silva, L.M. Cabral, A.K. Jordão, A.C. Cunha, M.C.B. Vieira, V.F. Ferreira, C.E. Carvalho-Pinto, H.C. Kang, H.C. Castro, In vitro and in vivo analysis of the antithrombotic and toxicological profile of new antiplatelets N-acylhydrazone derivatives and development of nanosystems: Determination of novel NAH derivatives antiplatelet and nanotechnological approach, *Thromb. Res.* 134 (2014) 376–383. doi: 10.1016/j.thromres.2014.05.009.
- [41] M. J. Parnham, H. Wetzig, Toxicity Screening of Liposomes, *Chem. Phys. Lipids* 64 (1993) 263–274. doi: 10.1016/0009-3084(93)90070-j.
- [42] M. Bauer, C. Lautenschlaeger, K. Kempe, L. Tauhardt, U.S. Schubert, D. Fischer, Poly(2-ethyl-2-oxazoline) as Alternative for the Stealth Polymer Poly(ethylene glycol): Comparison of in vitro Cytotoxicity and Hemocompatibility, *Macromol. Biosci.* 12 (2012). 986-998. doi:10.1002/mabi.201200017.
- [43] T. Mosmann, Rapid Colorimetric Assay for Cellular Growth and Survival: Application to Proliferation and Cytotoxicity Assays, *J. Immunol. Methods* 65 (1983) 55–63. doi: 10.1016/0022-1759(83)90303-4.
- [44] W.A. Da Silva, L.C. Da Silva, V.R. Campos, M.C. De Souza, V.F. Ferreira, Â.C. Dos Santos, P.C. Sathler, G.S. De Almeida, F.R. Dias, L.M. Cabral, R.B. De Azeredo, A.C. Cunha, Synthesis and antitumor evaluation of hybrids of 5,8-dioxo-5,8-dihydroisoquinoline-4-carboxylates and carbohydrates, *Future Med. Chem.* 10 (2018). 527-540. doi: 10.4155/fmc-2017-0173.
- [45] D. M. Maron, B. N. Ames, Revised Methods for the Salmonella Mutagenicity Test, *Mutat. Res. Mutagen. Relat. Subj.* 113 (1983) 173–215. doi: 10.1016/0165-1161(83)90010-9.
- [46] G. Muratore, B. Mercorelli, L. Goracci, G. Cruciani, P. Digard, G. Palù, A. Loregian, Human cytomegalovirus inhibitor AL18 also possesses activity against influenza A and B

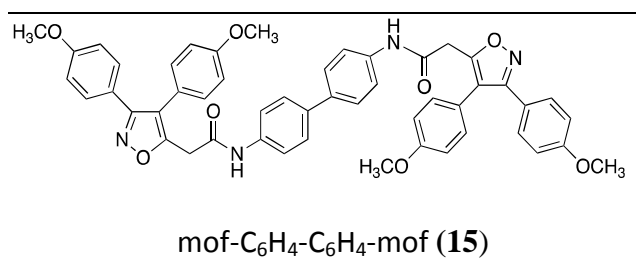
- viruses, *Antimicrob. Agents Chemother.* 56 (2012) 6009–6013. doi:10.1128/AAC.01219-12.
- [47] G. Cruciani, F. Milletti, L. Storchi, G. Sforna, L. Goracci, In silico pKa prediction and ADME profiling, *Chem. Biodivers.*, 6 (2009) 1812-1821. doi:10.1002/cbdv.200900153.
- [48] E. Carosati, S. Sciabola, G. Cruciani, Hydrogen bonding interactions of covalently bonded fluorine atoms: from crystallographic data to a new angular function in the GRID force field, *J. Med. Chem.* 47 (2004) 5114–5125. doi:10.1021/jm0498349.

Journal Pre-proof

Table 1. COX inhibitory activity of mof-spacer-mof molecules (**9-15**) bearing different spacers (**2-8**).

Journal Pre-proof

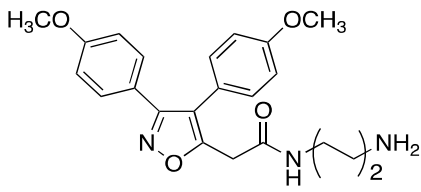
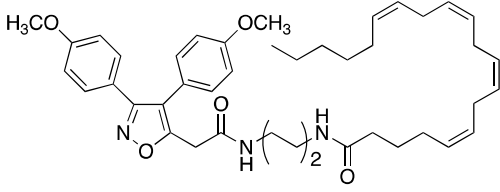
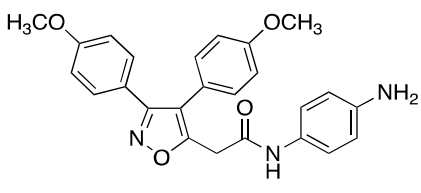
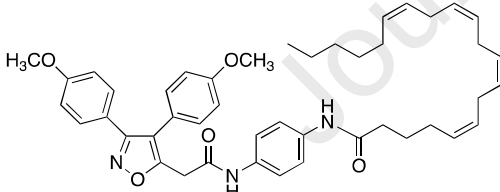
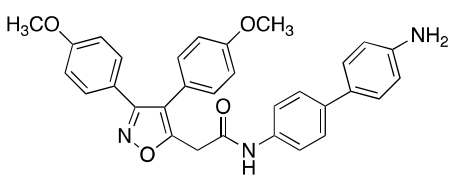
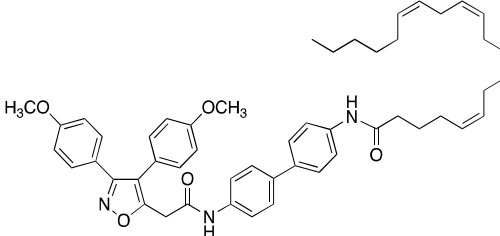
Compound	IC ₅₀ (μM) ^a (% inhibition) ^b		SI ^c	MW	cLogP ^c
	COX-1	COX-2			
 mofezolac (mof) (1)	0.0079 ± 0.15	>50	6392	339.11	2.51
 n = 1, spacer = -(CH ₂) ₂ - (mof-C ₂ -mof) (9)	0.013±0.0003 (75)	0.12±0.002 (45)	9	702.75	4.19
n = 2, spacer = -(CH ₂) ₄ - (mof-C ₄ -mof) (10)	5.5±0.1 (74)	>50	> 9	730.30	3.94
n = 3, spacer = -(CH ₂) ₆ - (mof-C ₆ -mof) (11)	9.0±0.2 (50)	>50	5.5	758.86	5.00
n = 6, spacer = -(CH ₂) ₁₂ - (mof-C ₁₂ -mof) (12)	7.1±0.3 (40)	>50	7	842.43	8.17
 mof-C ₆ H ₄ -mof (13)	0.15±0.04 (85)	>50	333	750.27	5.45
 mof-CH ₂ C ₆ H ₄ CH ₂ -mof (14)	>50 ^d	>50 ^d	-	778.30	5.49

 <p style="text-align: center;">mof-C₆H₄-C₆H₄-mof (15)</p>	0.08±0.001 (73)	>50	625	826.30	7.34
------------------------------------------------------------------------------------------------------------------------------------------------------------------------------------------------	-----------------	-----	-----	--------	------

^aIC₅₀ values are the means of at least three independent measurements. ^bInhibition percentage (%) determined at the highest final inhibitor concentration used (50 μM). ^cSelectivity Index (SI) = COX-2 IC₅₀/COX-1 IC₅₀. ^dMeasured by using ChemBio3D Ultra.

Journal Pre-proof

Table 2. COX inhibitory activity of compounds composed by mofezolac and arachidonic acid (**19-21**) and their precursors (mofezolac linked to the spacers) (**16-18**).

Compound	IC ₅₀ (μM) ^a (% inhibition) ^b		SI ^c (1/SI)	MW	cLogP ^d
	COX-1	COX-2			
 mof-C₄-NH₂ (16)	0.95±0.01 (100)	3.5±0.12 (51)	3.7 (0.27)	409.20	1.49
 mof-C₄-AA (19)	16.0±0.2 (57)	0.8±0.02 (61)	0.05 (20)	695.43	8.66
 mof-C₆H₄-NH₂ (17)	24.0±0.9 (74)	0.5±0.0 (79)	0.02 (48)	429.17	2.57
 mof-C₆H₄-AA (20)	0.05±0.002 (66)	>50	> 1,000 (> 0.001)	715.40	10.44
 mof-C₆H₄-C₆H₄-NH₂ (18)	0.075±0.002 (85)	0.3±0.01 (71)	4 (0.25)	505.20	4.46
 mof-C₆H₄-AA (21)	17±0.7 (50)	0.09±0.003 (60)	0.005 (189)	791.43	12.29

mof-C ₆ H ₄ -C ₆ H ₄ -AA (21)					
------------------------------------------------------------------------------------	--	--	--	--	--

^aIC₅₀ values are the means of at least three independent measurements. ^bInhibition percentage (%) determined at the highest final inhibitor concentration used (50 μM). ^cSelectivity Index (SI) = COX-2 IC₅₀/COX-1 IC₅₀. ^dMeasured by using ChemBio3D Ultra.

Journal Pre-proof

Table 3. Antiplatelet profile of compounds on *in vitro* platelet aggregation of human citrated platelet rich plasma induced by arachidonic acid (AA).

Compound	IC ₅₀ (μM) ^a
mof-C ₆ H ₄ -mof (13)	0.91 ± 0.28
mof-C ₆ H ₄ -C ₆ H ₄ -mof (15)	0.44 ± 0.13
mof-C ₆ H ₄ -AA (20)	0.61 ± 0.24
mof-C ₆ H ₄ -C ₆ H ₄ -AA (21)	0.76 ± 0.16
mofezolac (1)	0.45 ± 0.04
Aspirin	1.11 ± 1.17

^aIC₅₀ = concentration at which 50% inhibition of platelet aggregation is observed.

Table 4. *In vitro* coagulation of human plasma (n = 3) activated by prothrombin time (PT) and thromboplastin time (APTT).^a

Compound (100μM)	PT (seconds)	APTT (seconds)
C -	13.9 \pm 0.8	44.8 \pm 1.5
C +	300 \pm 0.0	300 \pm 0.0
mof-C ₆ H ₄ -mof (13)	15.5 \pm 0.0	47.5 \pm 0.4
mof-C ₆ H ₄ -C ₆ H ₄ -mof (15)	15.1 \pm 0.3	46.5 \pm 1.1
mof-C ₆ H ₄ -AA (20)	15.3 \pm 1.0	55.6 \pm 1.2
mof-C ₆ H ₄ -C ₆ H ₄ -AA (21)	14.6 \pm 0.5	48.0 \pm 1.6
mofezolac (1)	14.2 \pm 0.3	50.8 \pm 0.23
Aspirin	14.6 \pm 1.0	50.3 \pm 0.3

^a(C-) = negative control: DMSO 1%. (C+) = positive control: 100 μ M rivaroxaban.

Table 5. Hemolytic profile of some representative novel isoxazoles through hemolysis assay.^a

Compound (100 μM)	Hemolysis (%)
C-	0.00 \pm 0.22
C+	100 \pm 2.01
mof-C ₆ H ₄ -mof (13)	0.00 \pm 0.04
mof-C ₆ H ₄ -C ₆ H ₄ -mof (15)	0.00 \pm 0.08
mof-C ₆ H ₄ -AA (20)	0.00 \pm 0.01
mof-C ₆ H ₄ -C ₆ H ₄ -AA (21)	0.14 \pm 0.08
mofezolac (1)	0.00 \pm 0.02
Aspirin	0.0 \pm 0.04

^a(C-) = 1% DMSO is the negative control; 1% Triton X-100 is the positive control (C+). Values below 10% are considered non hemolytic.

Table 6. Vero cells viability after 48 hours of exposition to the tested novel compounds at 10 and 100 μM .^a

Compounds	[μM]	Cell viability (%)	\pm S.D. (%)
Control	-	100	2.6
mof-C ₆ H ₄ -mof (13)	100	97	2.8
	10	98	0.5
mof-C ₆ H ₄ -C ₆ H ₄ -mof (15)	100	92	2.8
	10	100	4.8
mof-C ₆ H ₄ -AA (20)	100	79	3.2
	10	93	2.8
mof-C ₆ H ₄ -C ₆ H ₄ -AA (21)	100	84	3.1
	10	94	4.2
mofezolac (1)	100	91	4.6
	10	97	3.7
Aspirin	100	95	2.0
	10	100	2.8

^aData are presented as mean of cell viability values (n = 4) \pm standard deviations.

Table 7. Mutagenic and genotoxic activity of molecules without metabolic activation.^a

Compound	Ames Test				SOS chromotest	
	<i>S. typhimurium</i>				<i>E. coli</i>	
	TA97	TA98	TA100	TA102	PQ35	PQ37
mof-C ₆ H ₄ -mof (13)	-	-	-	-	-	-
mof-C ₆ H ₄ -C ₆ H ₄ -mof (15)	-	-	-	-	-	-
mof-C ₆ H ₄ -AA (20)	-	-	-	-	-	-
mof- C ₆ H ₄ -C ₆ H ₄ -AA (21)	-	-	-	-	-	-
mofezolac (1)	-	-	-	-	-	-
4-NQO	+	+	+	+	+	+
DMSO	-	-	-	-	-	-
Aspirin	-	-	-	-	-	-

^aAssays performed by dissolving the tested compounds in DMSO. 4-NQO was used as a positive control. Reported results derive by three different concentrations (10 μ M, 100 μ M and 500 μ M).

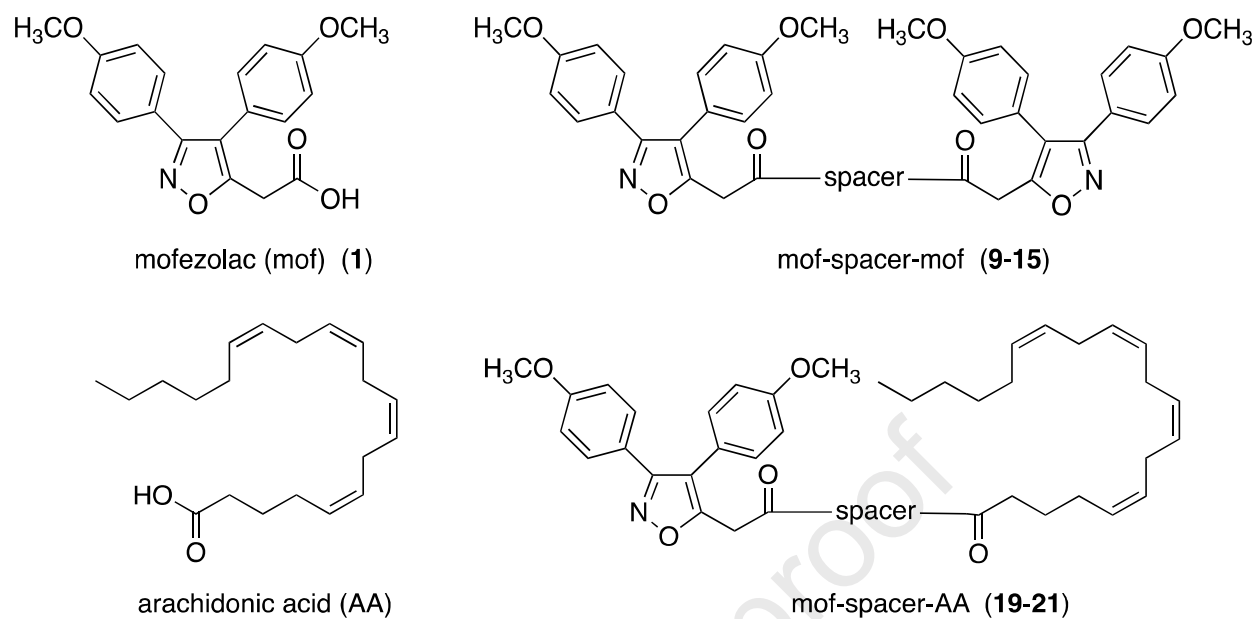


Figure 1. Chemical structures of mofezolac, arachidonic acid and two sets of novel isoxazoles (mofezolac-spacer-mofezolac and mofezolac-spacer-AA).

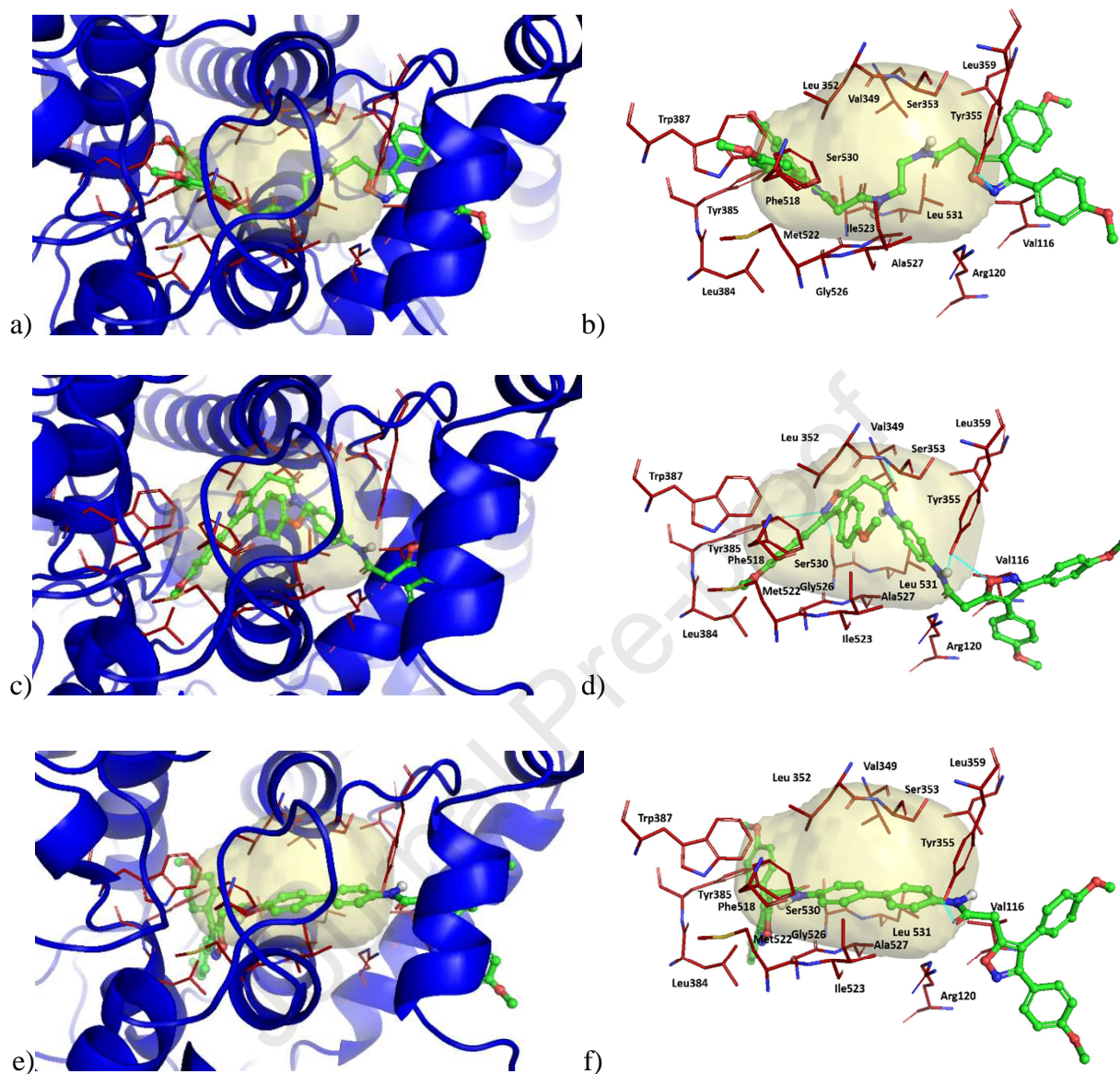


Figure 2. Proposed 3D binding mode inside the active site of COX-1, determined by FLAP analysis, for **9** (a, b), **13** (c, d) and **15** (e, f). Some of the COX-1 key residues located in the cavity are highlighted in stick-mode.

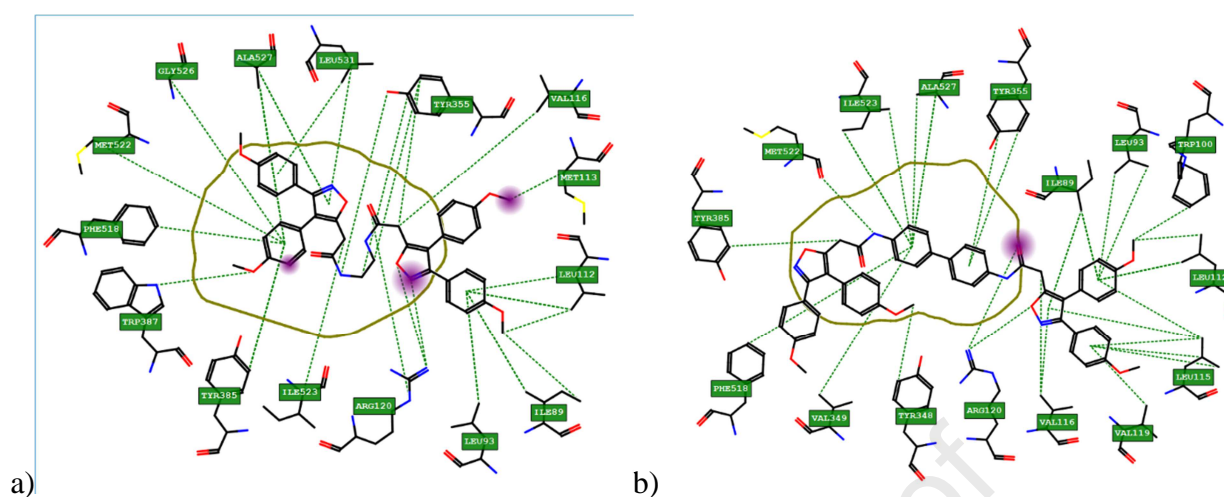


Figure 3. Comparison of the 2D FLAP binding poses for **9** (a) vs **15** (b). The most important COX-1 residues are shown together with their respective numbers. Purple regions indicate strong interactions.

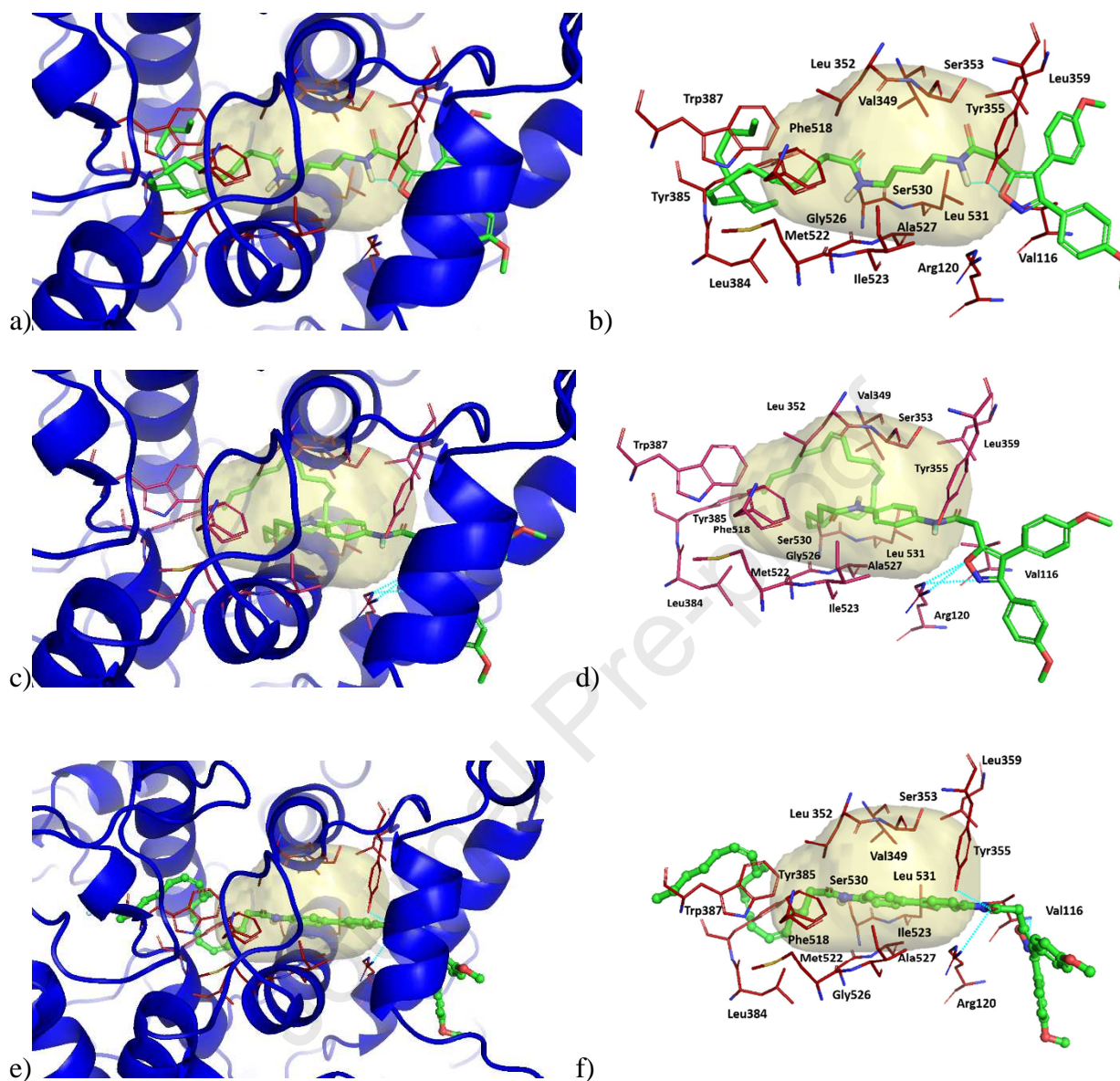


Figure 4. Proposed 3D binding mode inside the active site of COX-1, determined from FLAP analysis, for **19** (a, b), **20** (c, d) and **21** (e, f). Some of the COX-1 key residues located in the cavity are highlighted in stick-mode.

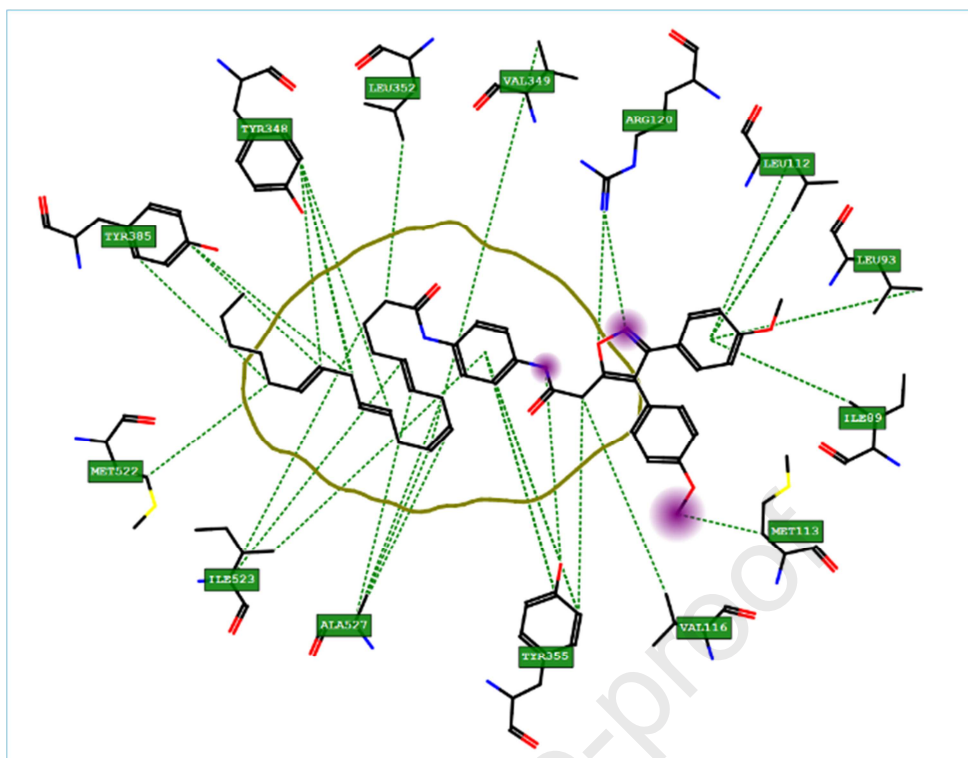


Figure 5. 2D FLAP binding pose of compound 20. The most important COX-1 residues are shown together with their respective numbers. Purple regions indicate strong interactions.

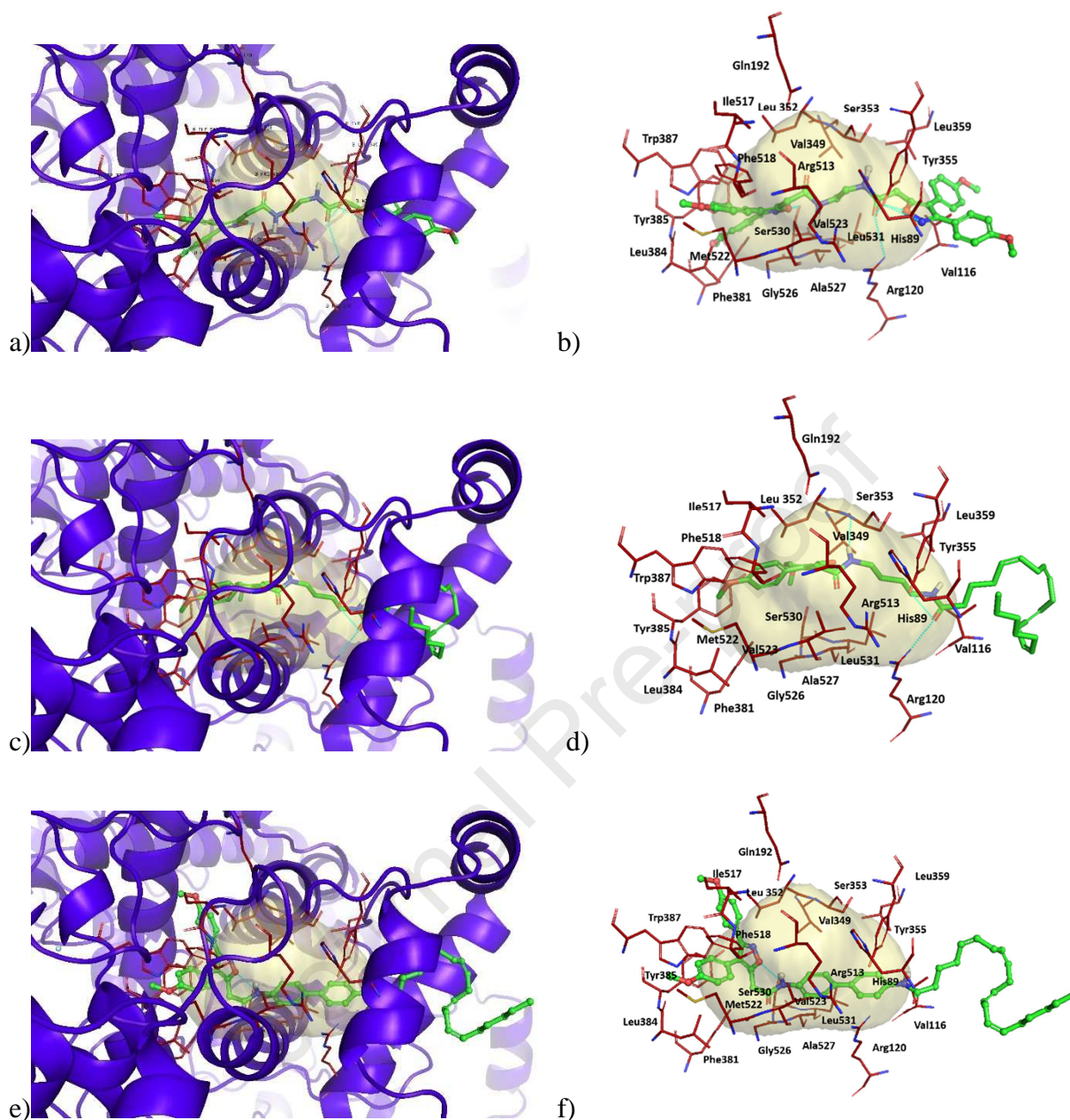


Figure 6. Proposed 3D binding mode inside the COX-2 active site determined by FLAP analysis for **9** (a, b), **19** (c, d) and **21** (e, f). Some of the COX-1 key residues located in the cavity are highlighted in stick-mode.

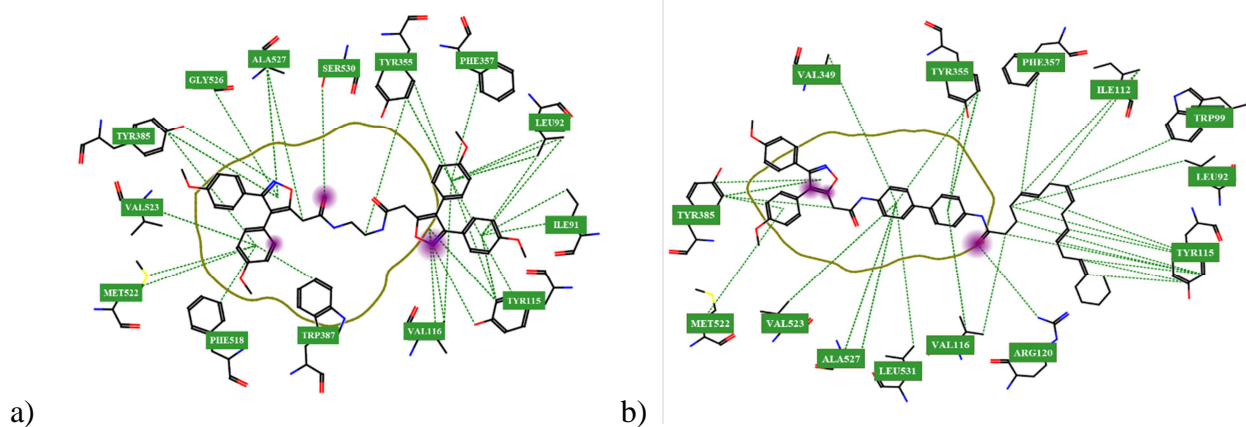
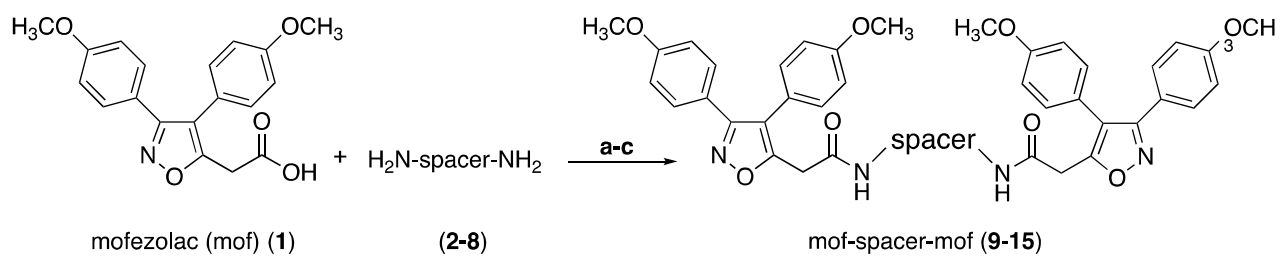
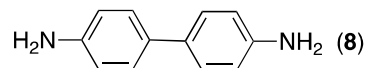
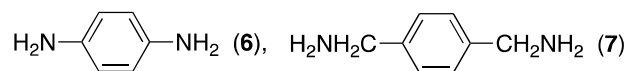
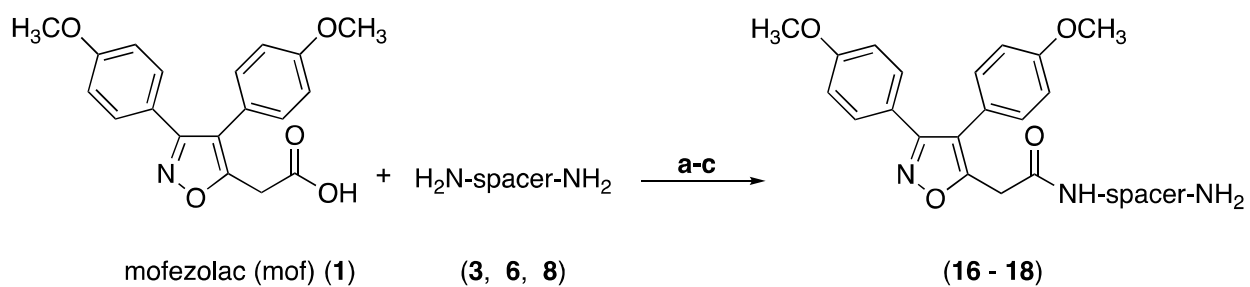


Figure 7. Comparison of the 2D FLAP binding poses for compounds **9** (a) vs **21** (b). The most important COX-2 residues are shown together with their respective numbers. Purple regions indicate strong interactions.

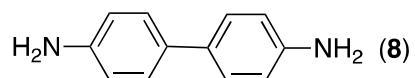
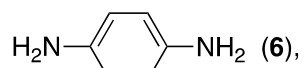


H₂N-spacer-NH₂ = H₂N(CH₂)₂NH₂ (2), H₂N(CH₂)₄NH₂ (3), H₂N(CH₂)₆NH₂ (4), H₂N(CH₂)₁₂NH₂ (5)

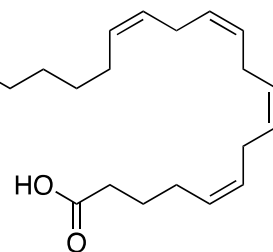




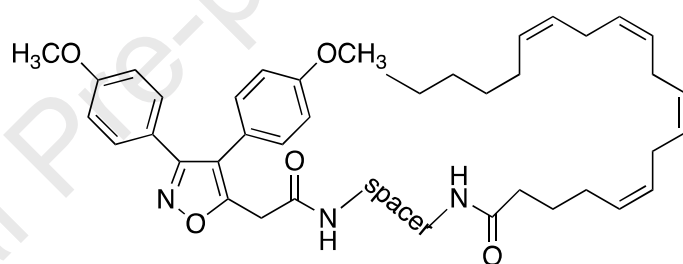
$\text{H}_2\text{N-spacer-NH}_2 = \text{H}_2\text{N}(\text{CH}_2)_4\text{NH}_2$ (**3***),



d-f



arachidonic acid (AA)



mof-spacer-AA (19 - 21)

Highlights

- Cross-talk between monomers of COX homodimers
- Double/hybrid inhibitors mofezolac-spacer-mofezolac and mofezolac-spacer-arachidonic acid were projected
- Molecular modelling by using FLAP algorithm shows fundamental interactions of the novel compounds at the entry channel of COX and inside its catalytic cavity
- Mof-spacer-mof and mof-spacer-AA inhibit *in vitro* free arachidonic acid-induced platelet aggregation. A positive profile of hemocompatibility in relation to their influence on the blood coagulation cascade and erythrocyte toxicity was also observed
- No Cytotoxicity and genotoxicity safety were also found for these two novel sets of compounds.

Declaration of interests

The authors declare that they have no known competing financial interests or personal relationships that could have appeared to influence the work reported in this paper.

Journal Pre-proof